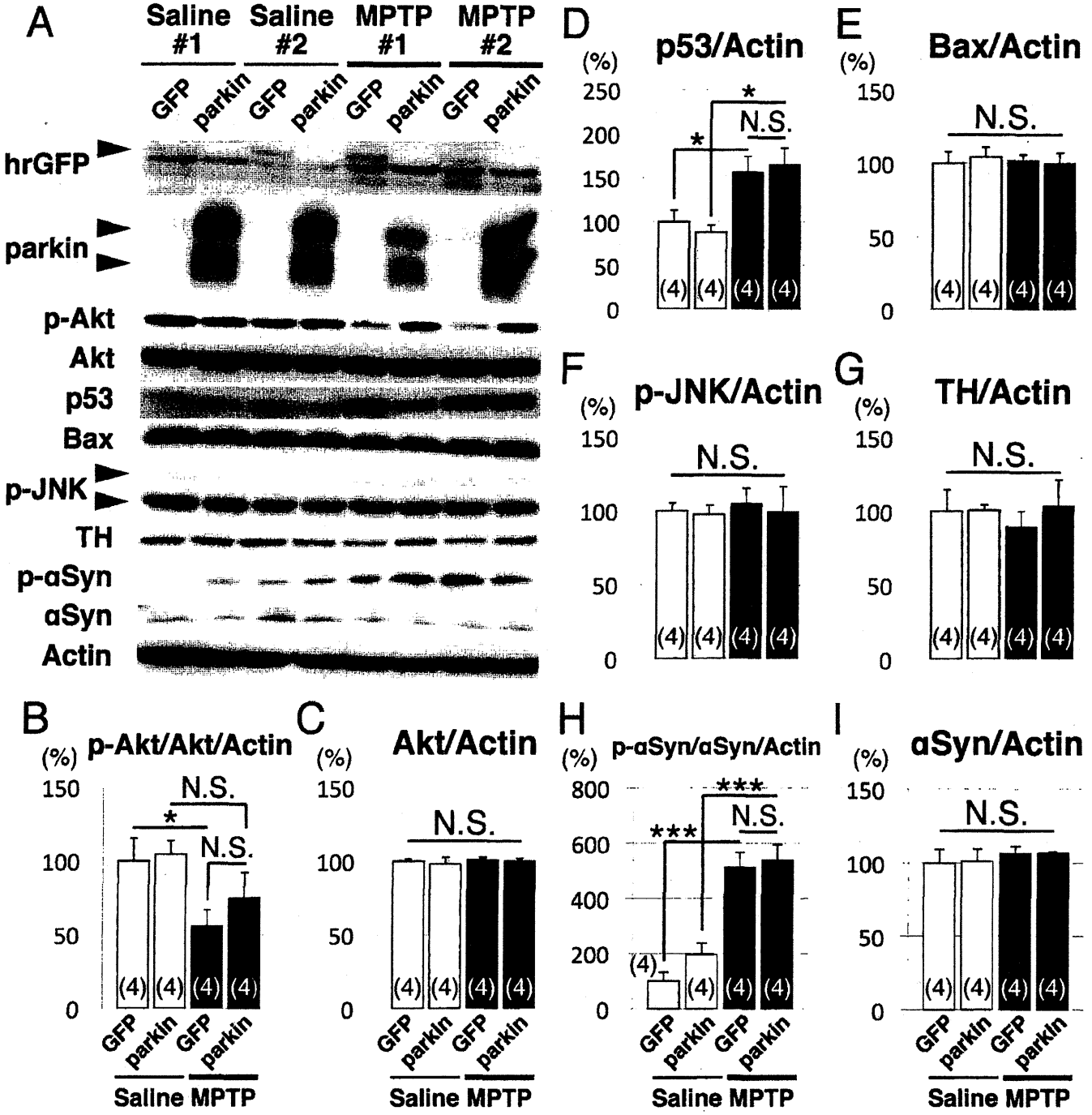

FIGURE 6. Proapoptotic and antiapoptotic molecules influenced by parkin overexpression in MPTP-minipump mice. **(A)** Western blotting was performed using midbrain tissues of mice killed 7 days after minipump implantation. Phosphorylated Akt (p-Akt) was reduced in the rAAV1-humanized recombinant green fluorescent protein (hrGFP)–injected side (GFP) but not in the rAAV1-parkin–injected side (parkin) of MPTP-minipump mice. **(B–G)** Data are presented as percentage of control (GFP/saline group) for p-Akt/Akt/Actin **(B)**, Akt/Actin **(C)**, p53/Actin **(D)**, Bax/Actin **(E)**, the phosphorylated JNK (p-JNK)/Actin **(F)**, tyrosine hydroxylase (TH)/Actin **(G)**, p-αSyn/αSyn/Actin **(H)**, and αSyn/Actin **(I)**. Reduction of p-Akt was significant in the rAAV1-hrGFP/MPTP group but not in the rAAV1-parkin/MPTP group. Total protein amount of Akt was unchanged. The protein levels of p53 and p-αSyn were significantly increased in the MPTP groups, and there were nonsignificant differences between the rAAV1-hrGFP/MPTP and rAAV1-parkin/MPTP groups. Numbers of mice analyzed in each group are indicated within the bars. Data are mean ± SEM. *, $p < 0.05$; and N.S., not significant (1-way analysis of variance followed by Tukey-Kramer post hoc test).

At 14 days after injection of the rAAV1 vectors, mice were implanted with minipumps to deliver MPTP at dose of 50 mg/kg per day (Fig. 3A; Table). Mice were examined for an apomorphine-induced rotation behavior 25 days after the treatment with MPTP. The injection of rAAV1-parkin resulted in increased contralateral turns in MPTP-minipump mice compared with rAAV1-parkin/saline ($p = 0.04633$; $df = 16$) and rAAV1-hrGFP/MPTP mice ($p = 0.02843$) (Fig. 3B). This suggests functional preservation of the nigrostriatal pathways provided by parkin delivery. Immunohistochemistry revealed overexpression of parkin in TH-positive DA cells in the SNpc (Figs. 3C–F; Figure, Supplemental Digital Content 1, parts 1C–M, http://links.lww.com/NEN/A252). Next, we counted TH- and Nissl-double-positive cells in the SNpc of these mice. As shown in Figures 3G to N and P, the injection of rAAV1 vector itself (i.e. in saline-treated groups) caused a minor decrease of DA cell number (15.1% ± 2.9% decrease in the rAAV1-hrGFP–injected mice and 7.9% ± 2.6% decrease in the rAAV1-parkin–injected mice). Importantly, rAAV1-parkin delivery promoted the survival of DA cell bodies in MPTP-minipump mice (109.0% ± 2.9% relative to the contralateral noninjected side) compared with parkin-overexpressed saline-minipump mice ($p = 0.005143$; $df = 16$) and hrGFP-overexpressed MPTP-minipump mice (88.0% ± 3.2%; $p = 0.0008401$) (Fig. 3P). The transduction efficiency of the rAAV1 vectors (i.e. the area immunopositive for parkin or hrGFP over the entire rostrocaudal area of the SNpc) varied from 87.5% ± 2.6% to 93.75% ± 3.6%, which had no statistical difference among the groups (Fig. 3O; Figure, Supplemental Digital Content 1, parts 1C-M, http://links.lww.com/NEN/A252). On the other hand, the striatal level of dopamine was not preserved with the injection of rAAV1-parkin, the same as with rAAV1-hrGFP (Fig. 4A). There was no influence on the striatal levels of dopamine metabolites, DOPAC and HVA, in these mice (Figs. 4B, C).

Accumulation of Ser129-Phosphorylated αSyn Promoted by Parkin Overexpression

There were increased numbers of p-αSyn–positive cell bodies in the rAAV1-parkin–injected side of the SN in MPTP-minipump mice (Figs. 5A–I). Thus, parkin delivery enhanced accumulation of the p-αSyn in DA cells in MPTP-minipump mice.

Alleviation of MPTP-Induced Inactivation of Akt by Parkin Delivery

On the basis of our previous report that showed upregulation of Bax 6 to 8 days after the first treatment with MPTP (30 mg/kg per day for 5 consecutive days) (41), we performed Western analyses at 7 days after minipump implantation (Fig. 3A). As shown in Figure 6, TH protein was slightly but nonsignificantly reduced by MPTP treatment and parkin counteracted the effect (Figs. 6A, G). There were no significant influences on the protein amounts of proapoptotic Bax (Figs. 6A, E) and the phosphorylated active form of JNK (Figs. 6A, F) in this model. The level of p53 was increased significantly in MPTP-minipump mice but had no significant difference between the rAAV1-hrGFP and rAAV1-parkin groups (Figs. 6A, D). Importantly, phosphorylated Akt, an active form of a prosurvival kinase Akt, was reduced in the rAAV1-hrGFP–injected hemisphere of MPTP-minipump mice ($p = 0.02829$; $df = 15$; compared with rAAV1-hrGFP/saline); the decrease was alleviated by rAAV1-parkin ($p = 0.8434$; compared with rAAV1-parkin/saline) (Figs. 6A, B). The level of total Akt protein was not changed by MPTP (Figs. 6A, C), indicating that parkin diminished the MPTP-induced dephosphorylation of p-Akt. p-αSyn was increased in response to MPTP ($p = 0.0001902$; $df = 15$; compared between rAAV1-hrGFP/saline and rAAV1-hrGFP/MPTP groups; and $p = 0.0009918$; compared between rAAV1-parkin/saline and rAAV1-parkin/MPTP groups), although there was no difference between the hrGFP and parkin groups at this time point ($p = 0.9780$; compared between rAAV1-hrGFP/MPTP and rAAV1-parkin/MPTP groups) (Figs. 6A, H). A similar result was obtained with another anti–p-αSyn antibody (clone pSyn#64; Wako; Figure, Supplemental Digital Content 3, part A, http://links.lww.com/NEN/A254). The total amount of αSyn protein was not changed by MPTP (Figs. 6A, I).

Effects of Parkin Overexpression on Mitochondrial Alterations

Finally, we addressed the effect of intranigral parkin delivery on the protein levels of PINK1 and a mitochondrial protein marker Tom20. Western blotting analysis demonstrated that both MPTP treatment and parkin expression rendered PINK1 to increase slightly but nonsignificantly (Figure, Supplemental Digital Content 3, parts A, B, http://links.lww.com/NEN/A254). The protein amounts of Tom20 and DJ-1 were not changed at this time point (Figure, Supplemental Digital Content 3, parts A, C, D, http://links.lww.com/NEN/A254). At day 28 after implantation of the minipumps, there was increased immunoreactivity for Tom20 in the SNpc of MPTP-minipump mice (Figure, Supplemental Digital Content 3, parts E-J, K-Z′, http://links.lww.com/NEN/A254); however, this phenomenon was not influenced by overexpression of parkin (Figure, Supplemental Digital Content 3, parts K-Z′, http://links.lww.com/NEN/A254). The overexpressed parkin was found scarcely colocalized with the mitochondrial Tom20 (Figure, Supplemental Digital Content 3, parts L-N′, P-R′, T-V′, and X-Z′, http://links.lww.com/NEN/A254).

DISCUSSION

In the present study, we generated a modified high-dose and long-term mouse model of PD using Alzet osmotic minipump administration of MPTP. In our preliminary experiments, we tried to produce an MPTP-minipump model according to the regimen of Fornai et al (39) but were unsuccessful. Alvarez-Fischer et al (42) recently demonstrated that an Alzet minipump-mediated infusion of MPTP alone (40 mg/kg per day for 3 weeks) caused only a transient depletion of the striatal dopamine and no DA cell loss in the SN. They further indicated that minipump-mediated infusion of MPTP (40–80 mg/kg per day for 2–4 weeks) in combination with the uricosuric agent probenecid caused moderate degeneration of DA neurons (42). We did not attempt to

inhibit renal excretion and/or brain efflux clearance of MPTP/MPP^+ but could generate a novel MPTP-minipump model by simply increasing the dose of MPTP to 50 and 100 mg/kg per day.

In this long-term environmental model of PD, we first evaluated the therapeutic effect of parkin. The rAAV vector was chosen because of its ability for long-term stable gene expression in postmitotic neurons with low accompanying cytotoxicities (43, 44). These properties are preferable for recent clinical trials to treat neurodegenerative disorders including PD (44, 45). Paterna et al (26) reported that rAAV vector–mediated transduction of parkin protected DA neurons of mice that were treated transiently with low dose of MPTP (20 mg/kg per day for 4 days). Our present data are in line with those results and indicate further that *parkin* gene therapy might be effective in a more severe and continuous condition causing PD. In 6-hydroxydopamine–lesioned rats, Vercammen et al (25) reported that lentiviral vector-parkin delivery resulted in a significant preservation of DA cell bodies and nerve terminals with corresponding behavioral improvement; by contrast, another group demonstrated that rAAV-parkin delivery ameliorated motor deficits but had no protection on the striatal DA innervation and nigral TH-positive neurons (46). In the present study, the MPTP-induced decrease of striatal dopamine was not prevented by rAAV1-parkin, whereas motor deficits and DA cell loss were ameliorated. We speculate that this discrepancy might be a result of an enhanced dopamine release of the surviving DA neurons that overexpress parkin (46), in consideration with an impaired dopamine release in parkin knockout mice (18).

We observed more the p-αSyn–immunopositive cells in the parkin-overexpressed SN of MPTP-minipump mice. There have been conflicting reports about the neurotoxicity of the p-αSyn in αSyn overexpression PD models; alteration of Ser129 to nonphosphorylated Ala or a phospho-mimetic Asp resulted in enhanced, eliminated, or unchanged the neurotoxicity of αSyn (47–51). Our present data imply that parkin delivery promoted DA neuronal survival in part by increasing the accumulation of the p-αSyn. This is consistent with the report by Gorbatyuk et al (48), who demonstrated that rAAV-mediated overexpression of αSyn Ser129Asp (which seemed to form punctate inclusions) caused no pathologic change in the SN. It has been speculated that parkin promoted accumulation of αSyn through catalyzing a nonclassic polyubiquitination of modified αSyn and/or αSyn-interacting proteins (13).

We found that MPTP-induced reduction of the phosphorylated active form of Akt was prevented by parkin overexpression. Recent work indicated that parkin potentiates epidermal growth factor (EGF)–induced activation of Akt signaling through interfering with Eps15, a negative regulator of the EGF/EGF receptor pathway (52). It is known that rAAV vector–mediated transduction of constitutively active form of Akt can provide DA neuroprotection in 6-hydroxydopamine mice (53). Moreover, Aleyasin et al (54) recently reported that DJ-1 (the loss-of-function mutations of which cause another form of recessively inherited PD) is necessary for Akt-mediated neuronal protection against MPTP. In agreement with these reports, our results suggest that maintenance of Akt signaling by parkin is important for the promotion of DA neuronal survival. On the other hand, da Costa et al (55) demonstrated that parkin elicits ubiquitin ligase-independent transcriptional repression of *p53* gene. In our present experiments, however, we did not find that ectopic parkin counteracted against the MPTP-induced upregulation of p53.

Parkin acts in concert with PINK1 in mitochondrial quality control (29–33). Overexpressed parkin interacts directly with and stabilizes PINK1 (56). Mitochondrial impairment also stabilizes PINK1, and recruitment of parkin to the damaged mitochondria is dependent on PINK1 in mitophagy (30, 31, 33). In the present study, the virally expressed parkin seemed not to affect the clearance of mitochondria that were damaged with MPTP treatment. These results suggest that a long-term insult makes it difficult for parkin to be effective in eliminating potentially harmful accumulated mitochondria.

In conclusion, the present study lends support to the hypothesis that the rAAV vector–mediated *parkin* gene therapy may have clinical benefits for advanced patients with idiopathic PD (16, 45, 57) and provides a new insight into the neuroprotective actions of multifunctional parkin in animal PD models.

ACKNOWLEDGMENT

The authors thank Hideki Shimura, MD, PhD, Department of Neurology, Juntendo University Urayasu Hospital, for his excellent advice.

REFERENCES

1. Farrer MJ. Genetics of Parkinson disease: Paradigm shifts and future prospects. Nat Rev Genet 2006;7:306–18
2. Shults CW. Lewy bodies. Proc Natl Acad Sci U S A 2006;103:1661–68
3. Dauer W, Przedborski S. Parkinson's disease: Mechanisms and models. Neuron 2003;39:889–909
4. Kitada T, Asakawa S, Hattori N, et al. Mutations in the *parkin* gene cause autosomal recessive juvenile parkinsonism. Nature 1998;392:605–8
5. Shimura H, Hattori N, Kubo S, et al. Familial Parkinson disease gene product, *parkin*, is a ubiquitin-protein ligase. Nat Genet 2000;25:302–5
6. Takahashi H, Ohama E, Suzuki S, et al. Familial juvenile parkinsonism: Clinical and pathologic study in a family. Neurology 1994;44:437–41
7. Mori H, Kondo T, Yokochi M. Pathologic and biochemical studies of juvenile parkinsonism linked to chromosome 6q. Neurology 1998;51: 890–92
8. Hayashi S, Wakabayashi K, Ishikawa A, et al. An autopsy case of autosomal-recessive juvenile parkinsonism with a homozygous exon 4 deletion in the *parkin* gene. Mov Disord 2000;15:884–88
9. van de Warrenburg BP, Lammens M, Lucking CB, et al. Clinical and pathologic abnormalities in a family with parkinsonism and *parkin* gene mutations. Neurology 2001;56:555–57
10. Savitt JM, Dawson VL, Dawson TM. Diagnosis and treatment of Parkinson disease: Molecules to medicine. J Clin Invest 2006;116:1744–54
11. Moore DJ. Parkin: A multifaceted ubiquitin ligase. Biochem Soc Trans 2006;34:749–53
12. Lim KL, Chew KC, Tan JM, et al. Parkin mediates nonclassical, proteasomal-independent ubiquitination of synphilin-1: Implications for Lewy body formation. J Neurosci 2005;25:2002–9
13. Lim KL, Dawson VL, Dawson TM. Parkin-mediated lysine 63–linked polyubiquitination: A link to protein inclusions formation in Parkinson's and other conformational diseases? Neurobiol Aging 2006;27:524–29
14. Doss-Pepe EW, Chen L, Madura K. alpha-Synuclein and *parkin* contribute to the assembly of ubiquitin lysine 63–linked multiubiquitin chains. J Biol Chem 2005;280:16619–24

15. Mukhopadhyay D, Riezman H. Proteasome-independent functions of ubiquitin in endocytosis and signaling. Science 2007;315:201–5
16. Yasuda T, Mochizuki H. The regulatory role of alpha-synuclein and *parkin* in neuronal cell apoptosis: Possible implications for the pathogenesis of Parkinson's disease. Apoptosis 2010;15:1312–21
17. Palacino JJ, Sagi D, Goldberg MS, et al. Mitochondrial dysfunction and oxidative damage in *parkin*-deficient mice. J Biol Chem 2004;279: 18614–22
18. Kitada T, Pisani A, Karouani M, et al. Impaired dopamine release and synaptic plasticity in the striatum of *parkin*−/− mice. J Neurochem 2009; 110:613–21
19. Frank-Cannon TC, Tran T, Ruhn KA, et al. Parkin deficiency increases vulnerability to inflammation-related nigral degeneration. J Neurosci 2008; 28:10825–34
20. Chung KK, Thomas B, Li X, et al. *S*-nitrosylation of parkin regulates ubiquitination and compromises *parkin*'s protective function. Science 2004;304:1328–31
21. Yao D, Gu Z, Nakamura T, et al. Nitrosative stress linked to sporadic Parkinson's disease: *S*-nitrosylation of parkin regulates its E3 ubiquitin ligase activity. Proc Natl Acad Sci U S A 2004;101:10810–14
22. LaVoie MJ, Ostaszewski BL, Weihofen A, et al. Dopamine covalently modifies and functionally inactivates parkin. Nat Med 2005;11:1214–21
23. Ng CH, Mok SZ, Koh C, et al. Parkin protects against LRRK2 G2019S mutant-induced dopaminergic neurodegeneration in *Drosophila*. J Neurosci 2009;29:11257–62
24. Yang Y, Gehrke S, Imai Y, et al. Mitochondrial pathology and muscle and dopaminergic neuron degeneration caused by inactivation of *Drosophila* Pink1 is rescued by Parkin. Proc Natl Acad Sci U S A 2006; 103:10793–98
25. Vercammen L, Van der Perren A, Vaudano E, et al. Parkin protects against neurotoxicity in the 6-hydroxydopamine rat model for Parkinson's disease. Mol Ther 2006;14:716–23
26. Paterna JC, Leng A, Weber E, et al. DJ-1 and Parkin modulate dopamine-dependent behavior and inhibit MPTP-induced nigral dopamine neuron loss in mice. Mol Ther 2007;15:698–704
27. Yamada M, Mizuno Y, Mochizuki H. Parkin gene therapy for alpha-synucleinopathy: A rat model of Parkinson's disease. Hum Gene Ther 2005;16:262–70
28. Yasuda T, Miyachi S, Kitagawa R, et al. Neuronal specificity of alpha-synuclein toxicity and effect of Parkin co-expression in primates. Neuroscience 2007;144:743–53
29. Whitworth AJ, Pallanck LJ. The PINK1/Parkin pathway: A mitochondrial quality control system? J Bioenerg Biomembr 2009;41:499–503
30. Vives-Bauza C, Zhou C, Huang Y, et al. PINK1-dependent recruitment of Parkin to mitochondria in mitophagy. Proc Natl Acad Sci U S A 2010; 107:378–83
31. Narendra DP, Jin SM, Tanaka A, et al. PINK1 is selectively stabilized on impaired mitochondria to activate Parkin. PLoS Biol 2010;8:e1000298
32. Geisler S, Holmstrom KM, Skujat D, et al. PINK1/Parkin-mediated mitophagy is dependent on VDAC1 and p62/SQSTM1. Nat Cell Biol 2010;12:119–31
33. Matsuda N, Sato S, Shiba K, et al. PINK1 stabilized by mitochondrial depolarization recruits Parkin to damaged mitochondria and activates latent Parkin for mitophagy. J Cell Biol 2010;189:211–21
34. Yamada M, Iwatsubo T, Mizuno Y, et al. Overexpression of alpha-synuclein in rat substantia nigra results in loss of dopaminergic neurons, phosphorylation of alpha-synuclein and activation of caspase-9: Resemblance to pathogenetic changes in Parkinson's disease. J Neurochem 2004; 91:451–61
35. Yasuda T, Nihira T, Ren YR, et al. Effects of UCH-L1 on alpha-synuclein over-expression mouse model of Parkinson's disease. J Neurochem 2009; 108:932–44
36. Przedborski S, Jackson-Lewis V, Naini AB, et al. The parkinsonian toxin 1-methyl-4-phenyl-1,2,3,6-tetrahydropyridine (MPTP): A technical review of its utility and safety. J Neurochem 2001;76:1265–74
37. Da Cunha C, Wietzikoski EC, Ferro MM, et al. Hemiparkinsonian rats rotate toward the side with the weaker dopaminergic neurotransmission. Behav Brain Res 2008;189:364–72
38. Furuya T, Hayakawa H, Yamada M, et al. Caspase-11 mediates inflammatory dopaminergic cell death in the 1-methyl-4-phenyl-1,2,3,6-tetrahydropyridine mouse model of Parkinson's disease. J Neurosci 2004; 24:1865–72
39. Fornai F, Schluter OM, Lenzi P, et al. Parkinson-like syndrome induced by continuous MPTP infusion: Convergent roles of the ubiquitin-proteasome system and alpha-synuclein. Proc Natl Acad Sci U S A 2005; 102:3413–18
40. Fujiwara H, Hasegawa M, Dohmae N, et al. alpha-Synuclein is phosphorylated in synucleinopathy lesions. Nat Cell Biol 2002;4:160–64
41. Cao XQ, Arai H, Ren YR, et al. Recombinant human granulocyte colony-stimulating factor protects against MPTP-induced dopaminergic cell death in mice by altering Bcl-2/Bax expression levels. J Neurochem 2006;99:861–67
42. Alvarez-Fischer D, Guerreiro S, Hunot S, et al. Modelling Parkinson-like neurodegeneration via osmotic minipump delivery of MPTP and probenecid. J Neurochem 2008;107:701–11
43. Burger C, Gorbatyuk OS, Velardo MJ, et al. Recombinant AAV viral vectors pseudotyped with viral capsids from serotypes 1, 2, and 5 display differential efficiency and cell tropism after delivery to different regions of the central nervous system. Mol Ther 2004;10:302–17
44. Mandel RJ, Manfredsson FP, Foust KD, et al. Recombinant adeno-associated viral vectors as therapeutic agents to treat neurological disorders. Mol Ther 2006;13:463–83
45. Mochizuki H, Yasuda T, Mouradian MM. Advances in gene therapy for movement disorders. Neurotherapeutics 2008;5:260–69
46. Manfredsson FP, Burger C, Sullivan LF, et al. rAAV-mediated nigral human parkin over-expression partially ameliorates motor deficits via enhanced dopamine neurotransmission in a rat model of Parkinson's disease. Exp Neurol 2007;207:289–301
47. Chen L, Feany MB. alpha-Synuclein phosphorylation controls neurotoxicity and inclusion formation in a *Drosophila* model of Parkinson disease. Nat Neurosci 2005;8:657–63
48. Gorbatyuk OS, Li S, Sullivan LF, et al. The phosphorylation state of Ser-129 in human alpha-synuclein determines neurodegeneration in a rat model of Parkinson disease. Proc Natl Acad Sci U S A 2008;105: 763–68
49. Azeredo da Silveira S, Schneider BL, Cifuentes-Diaz C, et al. Phosphorylation does not prompt, nor prevent, the formation of alpha-synuclein toxic species in a rat model of Parkinson's disease. Hum Mol Genet 2009; 18:872–87
50. Chen L, Periquet M, Wang X, et al. Tyrosine and serine phosphorylation of alpha-synuclein have opposing effects on neurotoxicity and soluble oligomer formation. J Clin Invest 2009;119:3257–65
51. McFarland NR, Fan Z, Xu K, et al. alpha-Synuclein S129 phosphorylation mutants do not alter nigrostriatal toxicity in a rat model of Parkinson disease. J Neuropathol Exp Neurol 2009;68:515–24
52. Fallon L, Belanger CM, Corera AT, et al. A regulated interaction with the UIM protein Eps15 implicates parkin in EGF receptor trafficking and PI(3)K-Akt signalling. Nat Cell Biol 2006;8:834–42
53. Ries V, Henchcliffe C, Kareva T, et al. Oncoprotein Akt/PKB induces trophic effects in murine models of Parkinson's disease. Proc Natl Acad Sci U S A 2006;103:18757–62
54. Aleyasin H, Rousseaux MW, Marcogliese PC, et al. DJ-1 protects the nigrostriatal axis from the neurotoxin MPTP by modulation of the AKT pathway. Proc Natl Acad Sci U S A 2010;107:3186–91
55. da Costa CA, Sunyach C, Giaime E, et al. Transcriptional repression of p53 by parkin and impairment by mutations associated with autosomal recessive juvenile Parkinson's disease. Nat Cell Biol 2009;11:1370–75
56. Shiba K, Arai T, Sato S, et al. Parkin stabilizes PINK1 through direct interaction. Biochem Biophys Res Commun 2009;383:331–35
57. Mochizuki H. Parkin gene therapy. Parkinsonism Relat Disord 2009;15: S43–45

EJN EUROPEAN JOURNAL OF NEUROSCIENCE

European Journal of Neuroscience, Vol. 34, pp. 1355–1367, 2011 doi:10.1111/j.1460-9568.2011.07873.x

MOLECULAR AND DEVELOPMENTAL NEUROSCIENCE

Postnatal development of tyrosine hydroxylase mRNA-expressing neurons in mouse neostriatum

Masao Masuda,[1,*] Masami Miura,[1] Ritsuko Inoue,[1] Michiko Imanishi,[2] Sachiko Saino-Saito,[3,†] Masahiko Takada,[2,‡] Kazuto Kobayashi[4] and Toshihiko Aosaki[1]

[1]Neuropathophysiology Research Group, Tokyo Metropolitan Institute of Gerontology, Itabashi, Tokyo, Japan
[2]Department of System Neuroscience, Tokyo Metropolitan Institute for Neuroscience, Fuchu, Tokyo, Japan
[3]Department of Anatomy and Cell Biology, Yamagata University School of Medicine, Yamagata, Japan
[4]Department of Molecular Genetics, Institute of Biomedical Sciences, Fukushima Medical University School of Medicine, Fukushima, Japan

Keywords: dopamine, green fluorescent protein, Parkinson's disease, striatum, tyrosine hydroxylase

Abstract

The striatum harbors a small number of tyrosine hydroxylase (TH) mRNA-containing GABAergic neurons that express TH immunoreactivity after dopamine depletion, some of which reportedly resembled striatal medium spiny projection neurons (MSNs). To clarify whether the TH mRNA-expressing neurons were a subset of MSNs, we characterized their postnatal development of electrophysiological and morphological properties using a transgenic mouse strain expressing enhanced green fluorescent protein (EGFP) under the control of the rat TH gene promoter. At postnatal day (P)1, EGFP-TH$^+$ neurons were present as clusters in the striatum and, thereafter, gradually scattered ventromedially by P18 without regard to the striatal compartments. They were immunonegative for calbindin, but immunopositive for enkephalin (54.5%) and dynorphin (80.0%). Whole-cell patch-clamp recordings revealed at least two distinct neuronal types, termed EGFP-TH$^+$ Type A and B. Whereas Type B neurons were aspiny and negative for the MSN marker dopamine- and cyclic AMP-regulated phosphoprotein of 32 kDa (DARPP-32), Type A neurons constituted 75% of the EGFP$^+$ cells, had dendritic spines (24.6%), contained DARPP-32 (73.6%) and a proportion acquired TH immunoreactivity after injections of 1-methyl-4-phenyl-1,2,3,6-tetrahydropyridine and 3-nitropropionic acid. The membrane properties and *N*-methyl-D-aspartate : non-*N*-methyl-D-aspartate excitatory postsynaptic current ratio of Type A neurons were very similar to MSNs at P18. However, their resting membrane potentials and spike widths were statistically different from those of MSNs. In addition, the calbindin-like, DARPP-32-like and dynorphin B-like immunoreactivity of Type A neurons developed differently from that of MSNs in the matrix. Thus, Type A neurons closely resemble MSNs, but constitute a cell type distinct from classical MSNs.

Introduction

The striatum is the largest nucleus of the basal ganglia that receives massive dopaminergic inputs from the substantia nigra pars compacta. Although the striatum is essentially dopaminoceptive, it has been repeatedly reported that the striatum itself contains neurons that potentially produce dopamine in humans (Ikemoto *et al.*, 1997; Porritt *et al.*, 2000; Cossette *et al.*, 2005), monkeys (Dubach *et al.*, 1987; Betarbet *et al.*, 1997; Palfi *et al.*, 2002; Tande *et al.*, 2006) and rats (Tashiro *et al.*, 1989a,b; Mura *et al.*, 2000; Lopez-Real *et al.*, 2003; Jollivet *et al.*, 2004). The intrinsic dopaminergic neuron is a new addition to the striatal neuronal population and, in addition, the neuron itself is heterogeneous and contains several distinct subtypes. Birth-dating studies using bromodeoxyuridine (BrdU) after 1-methyl-4-phenyl-1,2,3,6-tetrahydropyridine (MPTP) injection revealed that these tyrosine hydroxylase (TH)-immunoreactive neurons resulted from a phenotypic shift of pre-existing GABAergic interneurons (Betarbet *et al.*, 1997; Mao *et al.*, 2001; Tande *et al.*, 2006). They are immunoreactive to the GABA-synthesizing enzyme glutamic acid decarboxylase (GAD) and are mostly immunonegative for calbindin, a Ca^{2+}-binding protein and a marker for the medium spiny projection neurons (MSNs) in the matrix compartment (Gerfen, 1992). In the mouse striatum, there are few cells, if any, that are immunoreactive for TH, but they do appear after dopamine depletion by a combined treatment of MPTP and 3-nitropropionic acid (3-NPA) (Nakahara *et al.*, 2001) or a 6-hydroxydopamine treatment (Darmopil *et al.*, 2008). These cells contain a small population of aspiny calretinin-positive neurons and a large number of aspiny and spiny neurons that express calbindin as well as enkephalin or dynorphin, markers for

Correspondence: Toshihiko Aosaki, as above.
E-mail: aosaki@tmig.or.jp

**Present address*: Department of Pharmaceutical Sciences, Tokyo Metropolitan Institute of Public Health, Shinjuku, Tokyo 169-0073, Japan.

†*Present address*: Yamagata Prefectural Kahoku Hospital, Kahoku, Yamagata 999-3511, Japan.

‡*Present address*: Systems Neuroscience Section, Primate Research Institute, Kyoto University, Inuyama, Aichi 484-8506, Japan.

Received 4 March 2011, revised 3 August 2011, accepted 9 August 2011

indirect or direct pathway MSNs, respectively, suggesting that there might be a population of MSNs that acquire TH immunoreactivity after dopamine depletion in rodents (Darmopil *et al.*, 2008).

In contrast, Ibanez-Sandoval *et al.* (2010) recently reported the first detailed electrophysiological characterization of TH-positive neurons in the adult mouse striatum of a bacterial artificial chromosome transgenic mouse strain that expresses enhanced green fluorescent protein (EGFP). They found at least four electrophysiologically distinct subtypes of EGFP-TH$^+$ neurons, none of which were retrogradely labeled by injection of rhodamine beads into both the globus pallidus and substantia nigra, indicating that they are aspiny TH$^+$/GABAergic interneurons.

These seemingly contradictory results prompted us to characterize the postnatal development of TH mRNA-expressing EGFP$^+$ neurons in transgenic mice harboring a 9-kb TH promoter/EGFP reporter construct, in order to contrast them with MSNs to see whether or not they constitute a distinct subset of MSNs (Sawamoto *et al.*, 2001; Matsushita *et al.*, 2002; Baker *et al.*, 2003). We report here that the most numerous developing EGFP-TH$^+$ neurons were aspiny or spiny GABAergic neurons that were immunoreactive for dynorphin, enkephalin and dopamine- and cyclic AMP-regulated phosphoprotein of 32 kDa (DARPP-32), some of which became electrophysiologically indistinguishable from MSNs late in development. However, their immunohistochemical and electrophysiological properties followed different developmental time courses compared with MSNs and their distribution was not constrained by the striosome-matrix borders, suggesting that they constitute a unique neuronal subtype distinct from classical, direct and indirect pathway MSNs in the striatum.

Materials and methods

Transgenic mice

Production of the TH-EGFP transgenic mice has been described in previous studies (Sawamoto *et al.*, 2001; Matsushita *et al.*, 2002). The transgene construct contained the 9.0-kb 5′-flanking region of the rat TH gene, the second intron of the rabbit β-globin gene, cDNA encoding EGFP (Clontech, Palo Alto, CA, USA) and polyadenylation signals of the rabbit β-globin and Simian virus 40 early genes. In the present study, the TH-EGFP/21–31 strain was used, and the strain was maintained by breeding to C57BL/6J inbred mice. Transgenic mice were identified by polymerase chain reaction amplification of the EGFP sequence from tail DNA. The Animal Care and Use Committee of the Tokyo Metropolitan Institute of Gerontology approved all experimental procedures using laboratory animals.

Immunohistochemistry

The anterior region of the striatum is developmentally distinct from the posterior region (Nery *et al.*, 2002). We examined the anterior part of the striatum in this study. Mice were deeply anesthetized with isoflurane and intracardially perfused with phosphate-buffered saline (PBS) followed by 4% paraformaldehyde solution in PBS. Brains were dissected from the mice and immersed in the same solution at 4 °C overnight. The fixed tissues were cut into sections (50 μm) with a ZERO 1 SuperMicroslicer (Dosaka, Kyoto, Japan). The multiple immunofluorescence technique was used to investigate colocalization of EGFP with other markers. Sections were blocked with 10% normal goat or donkey serum and 0.3% Triton X-100 in PBS for 1 h, and then incubated for 24 h with primary antibodies at 4 °C. Antibodies presented here were as follows: rabbit anti-TH polyclonal antibody (1 : 400; Chemicon, Temecula, CA, USA), rabbit anti-choline acetyltransferase antibody (1 : 400; Chemicon), rabbit anti-calretinin polyclonal antibody (1 : 400; Swant, Bellizona, Switzerland), goat anti-calretinin polyclonal antibody (1 : 2000; Chemicon), rabbit anti-calbindin D-28k monoclonal antibody (1 : 500; Chemicon), rabbit anti-GAD65/67 polyclonal antibody (1 : 500; Sigma-Aldrich, St Louis, MO, USA), rabbit anti-DARPP-32 polyclonal antibody (1 : 100; Chemicon), mouse anti-DARPP-32 antibody (1 : 125; BD Biosciences PharMingen, San Diego, CA, USA), rabbit anti-Met-enkephalin antibody (1 : 250; Biomol, Hamburg, Germany), rabbit anti-dynorphin B antibody (1 : 250; Bachem, Bubendorf, Switzerland), rat anti-green fluorescence protein (GFP) monoclonal antibody (1 : 500; Nacalai Tesque, Kyoto, Japan), mouse anti-Neuronal Nuclei (NeuN) monoclonal antibody (1 : 500; Chemicon), rabbit anti-TuJ1 polyclonal antibody (1 : 2000; Covance, Emeryville, CA, USA) and goat anti-doublecortin polyclonal antibody (1 : 500; Santa Cruz Biotechnology, Santa Cruz, CA, USA). After the sections had been washed with PBS containing 0.1% normal goat or donkey serum, 1% bovine serum albumin and 0.3% Triton X-100, they were incubated with Alexa Fluor 488-, 647- or Cy3-conjugated anti-rabbit, anti-mouse or anti-goat IgG secondary antibody or Cy3-conjugated streptavidin (Molecular Probes, Eugene, OR, USA; Jackson ImmunoResearch Inc., West Grove, PA, USA). The sections were washed with PBS containing 1% normal goat or donkey serum, 1% bovine serum albumin and 0.3% Triton X-100, and mounted in Aquatex (Merck, Darmstadt, Germany). In some experiments, Triton X-100 was omitted because the detergent disturbed GAD immunostaining of somatic profiles (Jinno & Kosaka, 2004). Low-magnification images were acquired using an MVX10 fluorescence microscope (Olympus, Tokyo, Japan) and high-resolution images were taken using an LSM 5 Pascal confocal laser scanning microscope equipped with a high numerical aperture oil-immersion objective lens (63×, NA 1.40, Zeiss, Oberkochen, Germany). Images were acquired as stacked files through the whole section thickness at an optimal step size (1.0 μm). Montages were made from maximum intensity projections of confocal z-stacks of EGFP-positive neurons. The contrast of digital images was enhanced with Adobe Photoshop (Adobe Systems Inc., San Jose, CA, USA).

Quantification of EGFP-positive neurons and EGFP-negative medium-sized neurons expressing calbindin-like, DARPP-32-like and dynorphin B-like immunoreactivity at postnatal day (P)2, P8 and P18–26 was carried out in randomly chosen areas in 2–4 randomly chosen striatal sections from 2 to 3 animals. The data are presented as a percentage of immunopositive or immunonegative cells out of all cells counted. Statistical analysis was performed using a chi-square test from a contingency table of the number of immunopositive and immunonegative cells, with the resultant graph shown in Fig. 4. The threshold for statistical significance was set at $P < 0.05$.

Electrophysiology

Whole brains taken from 2- to 20-day-old EGFP-TH$^+$ transgenic mice under anesthesia were placed in ice-cold artificial cerebraspinal fluid (CSF) containing the following (in mM): 124 NaCl, 3 KCl, 1 NaH_2PO_4, 1.2 $MgCl_2$, 2.4 $CaCl_2$, 10 glucose, buffered to pH 7.4 with $NaHCO_3$ (26 mM) saturated with 95% O_2 and 5% CO_2. Parasagittal or coronal slices (250 μm thick), cut using a Pro 7 Linear Microslicer (Dosaka), were continuously perfused with artificial CSF at a rate of 1–2 mL/min at 30 °C. Whole-cell patch-clamp recordings were collected by an EPC9/2 amplifier (Heka Elektronik, Lambrecht/Pfalz, Germany), with infrared differential contrast and fluorescent visualization using a BX50WI microscope (Olympus) with two charge-coupled device cameras (Hamamatsu Photonics, Shizuoka,

Japan and Dage-MTI, Michigan City, IN, USA). Patch pipettes (4–6 MΩ) were fabricated from borosilicate glass capillaries (1.5 mm o.d., 1.17 mm i.d.; Harvard Apparatus Ltd, Holliston, MA, USA) on a PC-10 puller (Narishige, Tokyo, Japan). For current- and voltage-clamp recordings, patch pipettes contained the following (in mM): 129 K-gluconate, 11 KCl, 2 $MgCl_2$, 10 HEPES, 4 Na_2-ATP, 0.3 GTP and 0.5% biocytin (brought to pH 7.3 with KOH; osmolarity, 280 mOsm). After obtaining a stable seal of > 1 GΩ, the whole-cell configuration was achieved by gentle suction. Data were corrected for a junction potential of −14 mV.

For electrophysiological characterization, responses were recorded in current-clamp mode evoked by current injections. Spike properties were calculated using the first spike evoked by a small suprathreshold current injection. Input resistance was determined by a −25 pA hyperpolarizing step from the resting membrane potential. The action potential onset was measured as the time point where the deflection of the curve was maximal. Time to peak and amplitude of afterhyperpolarization were measured from the action potential onset. Spike widths were measured at half amplitude, on action potentials induced by a depolarizing pulse with threshold strength for spike initiation.

The *N*-methyl-D-aspartate (NMDA) : non-NMDA current ratios were measured using the area under the first 150 ms of the excitatory postsynaptic current (EPSC) following the stimulus artifact. The control EPSC was obtained at a holding potential of −70 mV in magnesium-free saline containing the $GABA_A$ receptor blocker SR-95531 (Sigma) at 5 μM. The stimulating glass electrode was placed in the striatum. After obtaining the control EPSC, non-NMDA EPSCs were obtained by application of the NMDA antagonist D-(−)-2-amino-5-phosphonopentanic acid (Sigma) at 25 μM. The NMDA current was calculated by subtracting the non-NMDA current from the control.

Histological procedures and morphological analysis

After electrophysiological recording, slices were fixed in phosphate-buffered 4% paraformaldehyde with 0.2% picric acid for 24 h at 4 °C. For visualization of biocytin-filled neurons, slices were incubated with an avidin–biotin peroxidase complex (1 : 100; Vector Laboratories, Burlingame, CA, USA) in 0.05 M Tris-buffered saline with 0.03% Triton X-100 overnight at 4 °C. After washing, the slices were reacted with 3,3′-diaminobenzidine tetrahydrochloride (0.02%) and H_2O_2 (0.003%) in Tris-buffered saline. Cell bodies, dendrites and projecting axons of stained neurons were reconstructed under a microscope attached to a camera lucida apparatus. After the reconstructed figures were captured by a digital scanner, they were retraced and digitized using Adobe Illustrator CS3 (Adobe Systems Inc.). Morphological variables were measured with a 100× oil-immersion objective lens (UPlanFl; NA 1.30; Olympus) attached to a BX51 light microscope (Olympus). Data were not corrected for tissue shrinkage.

Dopamine depletion and bromodeoxyuridine labeling

Both 3-NPA (200 mg/kg, s.c.; Sigma) and MPTP-HCl (5 mg/kg, i.p.; Sigma) were administered in transgenic mice at 2 months of age. MPTP injections were subsequently performed seven times at 12 h intervals. Control mice were treated with saline. To label mitotic cells, these mice were also injected with BrdU (300 mg/kg, i.p.; Sigma) once a day for 10 days. Mice were anesthetized at day 7 after the last MPTP injection, and killed by transcardial perfusion with PBS followed by 4% paraformaldehyde in PBS. The brains were removed and fixed for immunohistochemistry. For detection of incorporated BrdU, DNA denaturation was performed by incubating sections in 2 M HCl solution (neutralized with 0.1 M sodium borate for 10 min) for 40 min at 40 °C. Mouse anti-BrdU monoclonal antibody (1 : 500; Chemicon) was used to visualize BrdU incorporation.

Statistics for electrophysiological analysis

Discriminant analysis was performed to identify the explanatory variables most valuable in predicting group membership of EGFP-positive neurons from the striatum of EGFP-TH^+ transgenic mice. Wilks' lambda statistic was used to detect differences between means of identified groups of EGFP-positive neurons and which variables contributed to their discrimination. Provided that the null hypothesis of homogeneity of variance–covariance matrices was supported, linear discriminant analysis was performed. When this was not the case, discriminant analysis using Mahalanobis distances (Mahalanobis, 1936) was implemented. Finally, we chose variables that generated discriminant functions with the highest correction rate.

Statistical significance was set at $P < 0.05$ and determined using Student's *t*-test, Mann–Whitney *U* test and one-way ANOVA followed by the Bonferroni corrected two-tailed *t*-test. All data are reported as mean ± SEM.

Results

Distribution and immunohistochemistry of EGFP-TH^+ neurons

A previous study by Baker *et al.* (2003) demonstrated that EGFP-positive cells in the striatum expressed TH mRNA but not protein in mice expressing EGFP under the control of the TH promoter. Using a transgenic mouse of the same strain at P1–18, we confirmed the result with confocal microscopy by counting only TH-immunoreactive cells with an identifiable unlabeled nucleus surrounded by TH-immunolabeled cytoplasm. No cells were immunostained for TH in the control mouse striatum (data not shown). However, EGFP-TH^+ cells were observed as early as P1 within the striatum as well as in the subcallosal streak (Fig. 1A). There is a tendency for the EGFP-TH^+ cells to spread more abundantly in the ventral striatum than in the dorsal striatum and some of them were in clusters at P1 (Fig. 1A′). Then, at P4–P18, the cells gradually dispersed in the ventromedial region (Fig. 1B″ and C″), and sparsely distributed in the dorsolateral region (Fig. 1B′ and C′) of the striatum.

We next examined whether EGFP-TH^+ cells in the striatum were colocalized with the mature neuronal marker NeuN, the immature neuronal marker TuJ1 and the migrating neuroblast marker doublecortin using P18 mouse brains (Francis *et al.*, 1999). All EGFP-TH^+ cells in the striatum of the transgenic mouse were immunoreactive for NeuN (data not shown) and some of them were also stained for TuJ1 (Fig. 2A). Doublecortin was also expressed in a subset of cells of the striatum (Fig. 2B, 17.8%, 140/786 cells). These results indicate that most of the cells are fully differentiated, but some are still immature and in the midst of migration (Francis *et al.*, 1999; Nacher *et al.*, 2001; Yang *et al.*, 2004).

To determine whether these EGFP-TH^+ neurons could be classified as classical striatal interneurons (Kawaguchi *et al.*, 1995), the slices were immunostained for choline acetyltransferase, neuronal nitric oxide synthase, parvalbumin and calretinin at P18. Although a small population of the neurons was found to be immunoreactive for calretinin (Fig. 2, 2.8%, 22/784), none were immunoreactive for choline acetyltransferase, neuronal nitric oxide synthase or parvalbumin (Fig. 2D and E, data not shown for calretinin and parvalbumin).

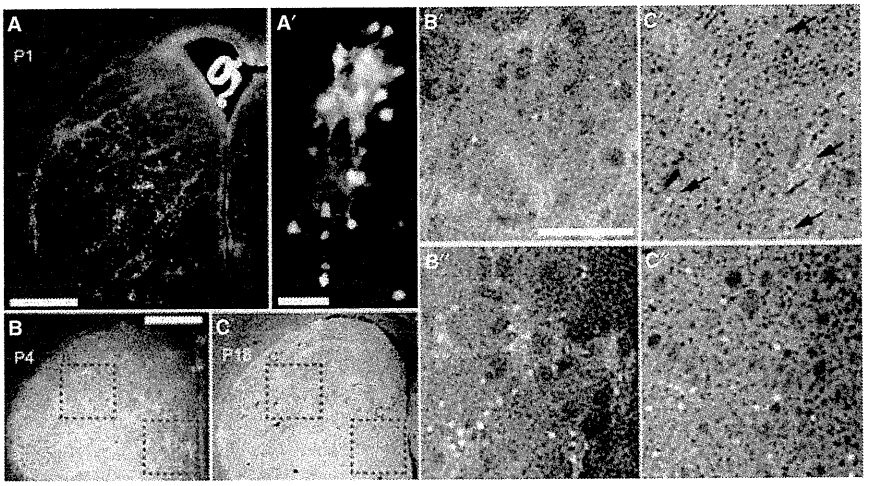

FIG. 1. Distribution patterns of EGFP$^+$ cells in coronal sections of the mouse striatum at P1 (A), P4 (B) and P18 (C). High-magnification images of red boxed areas in A, B and C are shown in A′, B′, B″, C′ and C″, respectively. Black arrows indicate the locations of EGFP-positive neurons in C′. EGFP-positive neurons were scattered in clusters in the ventral region at P1 and gradually dispersed at P4 and P18. EGFP$^+$ neurons were distributed mainly in the ventromedial striatum at P4 and P18. Scale bar: A, 500 μm; A′, 50 μm; (in B) B and C, 500 μm; (in B′) B′, B″, C′ and C″, 200 μm.

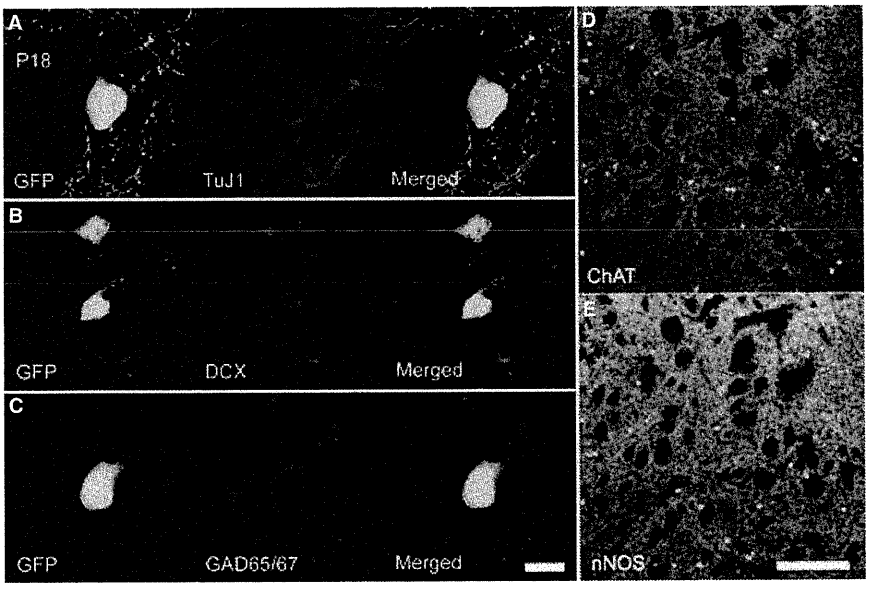

FIG. 2. Immunohistochemistry of EGFP$^+$ neurons in the striatum of 18-day-old transgenic mice. EGFP$^+$ neurons were colocalized with the immature neuronal marker TuJ1 (A) and the migrating neuroblast marker doublecortin (DCX) (B). EGFP$^+$ neurons expressed the GABA-synthesizing enzyme GAD65/67 (C), but no EGFP$^+$ neurons (green) in the striatum were immunopositive for choline acetyltransferase (ChAT) (red, D) and neuronal nitric oxide synthase (nNOS) (red, E). Scale bars: 10 μm in green fluorescent protein (GFP), GAD65/67, TuJ1 and DCX; 200 μm in ChAT and nNOS.

EGFP-TH$^+$ neurons also exhibited immunoreactivity for GAD65/67 (90.4%, 734/812, Fig. 2C) and DARPP-32 (73.6%, 590/802, see Fig. 6A) but not calbindin at P18. EGFP-TH$^+$ neurons were distributed widely in calbindin-sparse and calbindin-rich regions of the striosomes and matrix, respectively (Fig. 3A) (Gerfen *et al.*, 1985). However, in 2-month-old mice we found some EGFP-positive neurons near the subventricular zone, which were coexpressed with calbindin and DARPP-32 (Fig. 3B), suggesting that some EGFP-TH$^+$ neurons might acquire the same chemical features as the matrix MSNs later in development. Interestingly enough, as reported by Darmopil *et al.* (2008), half of the EGFP-TH$^+$ neurons were found to be immunoreactive to enkephalin (30/55, 54.5%), which is a marker for indirect pathway MSNs, and most contained dynorphin (56/70, 80.0%), a marker for direct pathway MSNs, even at P18 (Fig. 3C). Although we did not perform double immunostaining using antibodies against enkephalin and dynorphin, these results suggest that a significant number of the cells contained both enkephalin and dynorphin, which is in sharp contrast with MSNs that are largely separated into enkephalin-containing striatopallidal and dynorphin-containing striatonigral neurons (Gerfen & Young, 1988). Therefore, from a neurochemical perspective, EGFP-TH$^+$ neurons at P18 are very similar to either MSNs or calretinin interneurons, as previously reported.

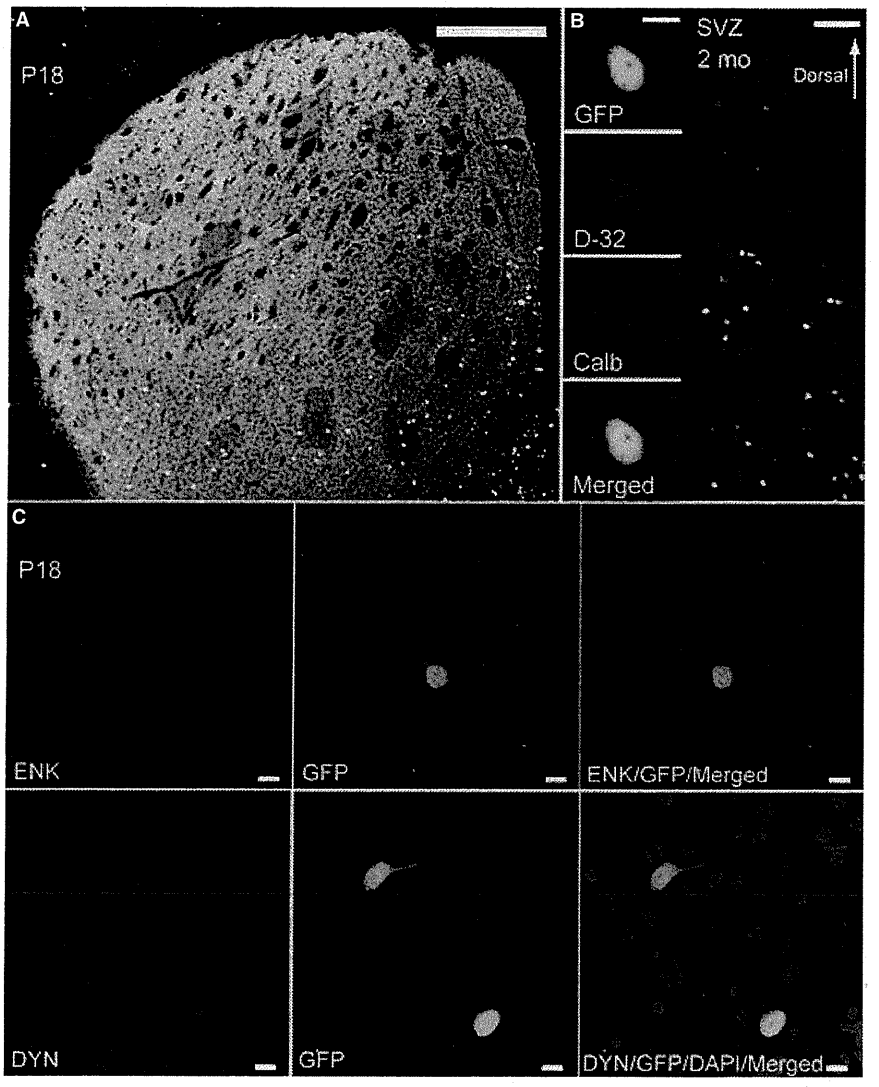

FIG. 3. EGFP$^+$ neurons ignore the compartmental boundaries. (A) EGFP$^+$ neurons exist in calbindin-sparse (striosomes) and calbindin-rich (matrix) regions of the striatum. Calbindin immunohistochemistry was used to identify the matrix compartment. Light red regions indicate calbindin-sparse striosomes and yellow dots denote EGFP$^+$ neurons located within the striosomes. (B) Colocalization of DARPP-32 (D-32) and calbindin (Calb) in an EGFP$^+$ neuron of a 2-month-old mouse (left panel). EGFP$^+$/calbindin$^+$ neurons (red dots) are located near the subventricular zone (SVZ) (right panel). (C) Colocalization of enkephalin (ENK) or dynorphin (DYN) in EGFP$^+$ neurons. Nuclear staining with 4′,6-diamidino-2-phenylindole (DAPI) was shown in a merged photo of a dynorphin-labeled slice. Scale bar: A, 500 μm; B, left panel, 10 μm; B, right panel, 100 μm; C, 10 μm; GFP, green fluorescent protein.

Postnatal development of calbindin-like, DARPP-32-like and dynorphin-like immunoreactivity of EGFP-TH$^+$ neurons as compared with medium spiny neurons

Because a population of EGFP-TH$^+$ neurons had similarities (immunoreactivity to DARPP-32, enkephalin and dynorphin) and dissimilarities (poor immunoreactivity to calbindin and seemingly indifferent to the striosome/matrix compartments) to MSNs at P18, we examined the postnatal development of calbindin-like, DARPP-32-like and dynorphin-like immunoreactivity of EGFP-TH$^+$ neurons at P2, P8 and P18–26. GFP-positive neuropil patches were identified as 'dopamine islands', precursors of the developing striosomal system, and the surrounding area was considered to be the matrix of the striatum. The numbers of medium-sized neurons and EGFP-TH$^+$ neurons in each area, in coronal sections at rostral and middle levels, were counted from photomicrographs of confocal images taken from 2 to 3 animals. Strictly speaking, the medium-sized neurons observed here were not identical to MSNs, but could be considered to be MSNs for the most part.

Calbindin-like immunoreactivity

At P2, dopamine islands, identified with EGFP-positive neuropil, were found scattered within the striatum and the surrounding matrix consisting of calbindin-poor and calbindin-rich zones (Liu and Graybiel, 1992a,b). In the matrix, 12.3% (20/162) and 96.4% (160/166) of the medium-sized neurons were calbindin-positive in the calbindin-poor and calbindin-rich zones, respectively. As a whole, 54.9% (180/328) of the medium-sized neurons in the matrix were calbindin-positive, whereas 86.7% (39/45) of those in the dopamine islands were calbindin-positive at P2 (Fig. 4B, upper). In contrast, 25.6% (41/160, Fig. 4B, white bar) of the EGFP-TH$^+$ neurons were

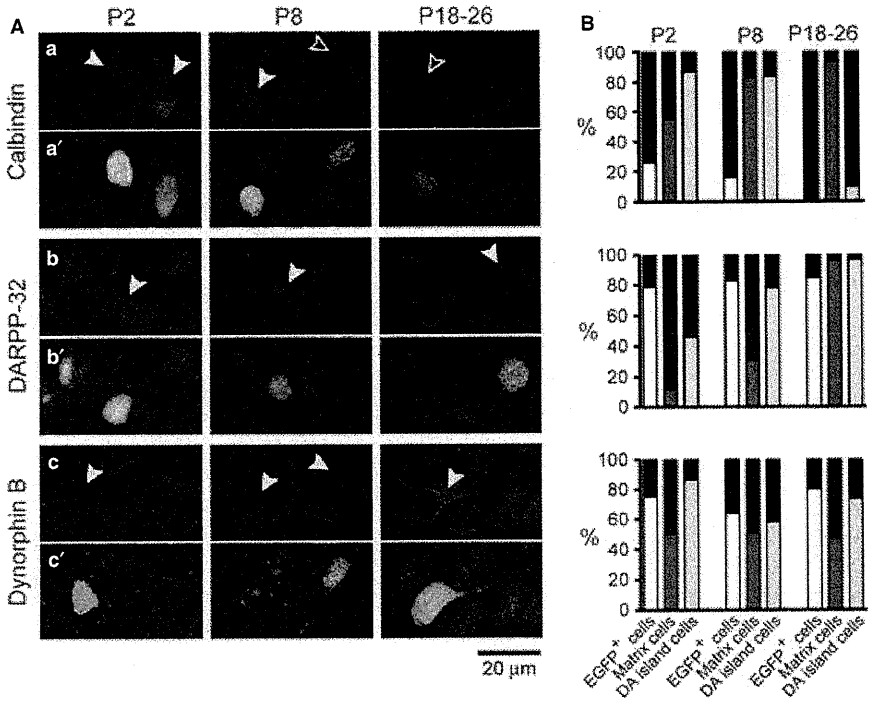

FIG. 4. Postnatal development of calbindin-like, DARPP-32-like and dynorphin B-like immunoreactivity in EGFP-TH$^+$ neurons and medium-sized neurons in dopamine islands and the matrix of the striatum. (A) Colocalization of calbindin, DARPP-32 and dynorphin B in EGFP-TH$^+$ neurons at P2, P8 and P26–28. Upper panels in each row (a, b and c) show calbindin-like, DARPP-32-like and dynorphin B-like immunoreactivity (shown in red), on which are superimposed nuclear staining with 4′,6-diamidino-2-phenylindole (DAPI, blue) and EGFP-TH$^+$ neurons (green) in the lower panels (a′, b′ and c′). Filled arrowheads indicate immunoreactive cells and open arrowheads indicate immunonegative cells. Scale bar: 20 μm. (B) The percentage of calbindin-like (upper), DARPP-32-like (middle) and dynorphin B-like (lower) immunoreactive cells in EGFP-TH$^+$ neurons (white), medium-sized neurons in the matrix (red) and medium-sized neurons in the dopamine (DA) islands (green) at P2, P8 and P18–26.

calbindin-positive. Additionally, 41.3% (66/160) of the EGFP-TH$^+$ neurons could be identified in either dopamine islands or the matrix. The islands contained 24.2% (16/66) of the cells with 62.5% (10/16) being calbindin-positive, whereas 26.0% (13/50) of the EGFP-TH$^+$ neurons in the matrix were calbindin-positive. Thus, at P2, a greater proportion of the cells located in dopamine islands were calbindin-positive compared with those in the matrix. At P8, the distinction between calbindin-rich and calbindin-poor regions in the matrix became obscure. As a whole, the percentage of calbindin-positive matrix cells increased to 82.7% (1266/1530) at P8 and 93.1% (861/925) at P26. In contrast, calbindin-positive cells in the dopamine islands dramatically decreased from 83.6% (275/329) at P8 to 9.4% (10/106) at P26, whereas the percentage of calbindin-positive cells in EGFP-TH$^+$ neurons decreased from 15.9% (14/88) at P8 to 1.9% (1/52) at P26. Statistical analyses indicated that EGFP-TH$^+$ neurons were different from both matrix cells and dopamine island cells with regard to calbindin-like immunoreactivity at P2 and P8 ($P < 0.0001$, chi-square test), whereas at P26, EGFP-TH$^+$ neurons were only different from matrix cells. EGFP-TH$^+$ neurons with calbindin-like immunoreactivity (filled arrowheads) and EGFP-negative cells without calbindin-like immunoreactivity (open arrowheads) are shown in Fig. 4Aa (calbindin, P2, P8 and P26).

DARPP-32-like immunoreactivity

It was previously reported that the amount of DARPP-32 protein increases throughout the first three postnatal weeks, peaks at P28 and then declines to plateau at adult levels (Ehrlich *et al.*, 1990). DARPP-32-like immunoreactivity was consistently weak in the matrix at P2 and P8 (Fig. 4Ab and Ab′, DARPP-32). The percentage of DARPP-32-positive medium-sized cells in the matrix was low at P2 (11.8%, 91/771) and P8 (30.3%, 91/300), but greatly increased to 96.5% (1761/1825) at P26. Dopamine islands tended to have more DARPP-32-positive medium-sized neurons than the matrix at P2 (45.9%, 237/516) and P8 (78.3%, 54/69), but at P26 the percentage of DARPP-32-positive cells was 96.6% (227/235), which was similar to that of cells in the matrix (Fig. 4B, DARPP-32). In sharp contrast, the percentage of DARPP-32-positive cells in EGFP-TH$^+$ neurons remained high throughout the four postnatal weeks (P2, 79.0%, 263/333; P8, 83.0%, 73/88; P26, 76.9%, 20/26). A significantly higher proportion of EGFP-TH$^+$ neurons were DARPP-32-positive at P2 and P8, but not at P26 ($P < 0.0001$, chi-square test).

We next examined the question of whether DARPP-32-positive or DARPP-32-negative neurons were unevenly distributed in the striatal compartments. We counted the number of DARPP-32-positive and DARPP-32-negative neurons in the dopamine islands and matrix. The island/matrix location of only 26 EGFP-TH$^+$ neurons could be identified, with 80.8% (21/26) located in the matrix and the remainder in dopamine islands. Of these cells, 76.2% (16/21) and 80.0% (4/5) were DARPP-32-positive in the matrix and dopamine islands, respectively, indicating that DARPP-32-positive neurons had no preference for either compartment.

Dynorphin B-like immunoreactivity

Dynorphin B-like immunoreactivity in the matrix was observed in about half of the matrix medium-sized cells throughout postnatal development (P2, 50.2%, 713/1421; P8, 51.0%, 321/629; P18, 47.6%, 364/764), whereas the dopamine islands contained a higher proportion of dynorphin-positive cells than the matrix (P2, 86.5%,

45/52; P8, 58.3%, 112/192; P18, 73.7%, 42/57). EGFP-TH$^+$ neurons were comprised of dynorphin-positive cells in 75.0% (117/156) at P2, 64.4% (159/247) at P8 and 80.0% (56/70) at P18 (Fig. 4A and B, Dynorphin B). Statistically, EGFP-TH$^+$ neurons contained a higher proportion of dynorphin-positive cells at P2, P8 and P18 ($P < 0.0001$) than matrix neurons. Overall, these results suggest that the developmental course of EGFP-TH$^+$ neurons was very different than that of striatal medium-sized, EGFP-negative neurons, in terms of histochemical features such as calbindin, DARPP-32 and dynorphin B immunoreactivity.

Electrophysiological properties of EGFP-TH$^+$ neurons

The EGFP-TH$^+$ neurons were recorded in whole-cell, current-clamp mode. All neurons sampled had resting membrane potentials more negative than −55 mV and overshooting spikes. Based on passive and active intrinsic properties revealed by intracellular current injection, these neurons were tentatively classified into two subtypes, EGFP-TH$^+$ Type A and Type B (Fig. 5A and B and Table 1).

Spontaneous spike discharge was observed in both types of neurons several minutes after breakage of patch membranes (Type A, 12.9%, 9/70; Type B, 75.0%, 12/16). The resting membrane potential of EGFP-TH$^+$ Type A neurons was −76.0 ± 0.9 mV (n = 131) and the input resistance was 406.0 ± 22.0 MΩ, whereas EGFP-TH$^+$ Type B neurons had a more depolarized resting membrane potential (−65.3 ± 0.8 mV, n = 37) and a higher input resistance (635.0 ± 54.0 MΩ) (Table 1, Fig. 5D). In EGFP-TH$^+$ Type A neurons, injection of negative current produced a small sag in the membrane potential (72.5%, 50/69, Fig. 5Aa, arrow). The response to depolarizing current injection was an initial action potential followed by a regular spiking train with a small adaptation (70.0%, 49/70). These neurons displayed slow afterhyperpolarization of 11.6 ± 0.5 mV (Fig. 5C, black trace). However, in 42.9% (12/28) of the cells examined, Type A neurons showed small depolarized plateau potentials upon release from depolarizing current injections (Fig. 5Ab, arrow), which were much smaller than those reported previously using brain slices taken from adult bacterial artificial chromosome transgenic mice (Ibanez-Sandoval *et al.*, 2010). The spiking threshold was −51.0 ± 0.5 mV and the spike amplitude was 78.0 ± 1.2 mV. Interestingly, delayed spiking due to a depolarizing ramp, in response to a depolarizing current pulse, was occasionally observed with inward rectification in Type A neurons in 4.3% (3/69), which made them indistinguishable from MSNs. However, EGFP-TH$^+$ Type B neurons exhibited a small sag upon hyperpolarizing current injection (53.3%, 8/15, Fig. 5Ba, arrow) and rebound spikes on release from a hyperpolarizing current step to depolarized resting potential (100%, 12/12, Fig. 5Ba, asterisk). They exhibited narrower spikes (spike widths at half amplitude, 0.68 ± 0.03 ms) and shorter afterhyperpolarization (3.4 ± 0.5 ms, Fig. 5B, red) than those of EGFP-TH$^+$ Type A neurons. Type B cells never exhibited depolarizing plateau potentials. A suprathreshold current injection induced fast, repetitive firing in EGFP-TH$^+$ Type B neurons and revealed a small adaptation of firing rate during repetitive discharges (31.3%, 5/16, Fig. 5Ba, red trace).

This broad classification into EGFP-TH$^+$ Type A and Type B neurons was statistically verified by discriminant analysis using resting membrane potential and spike width. Discriminant analysis was performed to determine the variables most valuable for predicting group membership of EGFP-positive neurons from EGFP-TH$^+$ transgenic mice. We selected a pair of electrophysiological properties as explanatory variables, and examined whether there were differences between Type A and Type B neurons and whether the variables

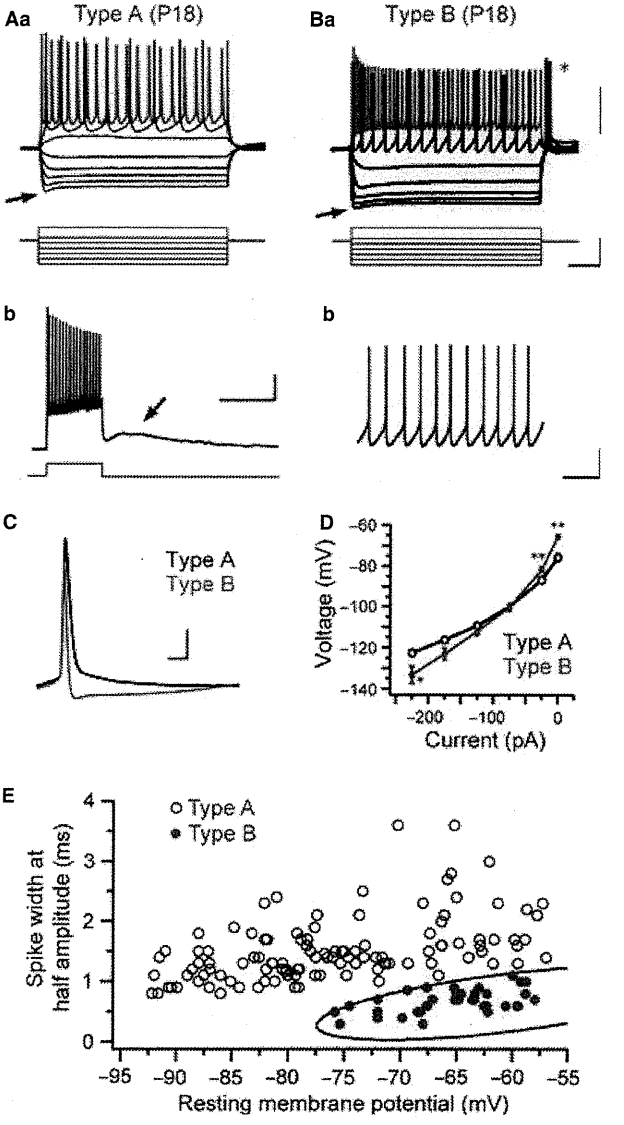

FIG. 5. Electrophysiological properties of EGFP-TH$^+$ Type A and B neurons. Subthreshold and suprathreshold responses of EGFP-TH$^+$ Type A and B neurons (P18) to hyperpolarizing and depolarizing current steps are shown in A and B, respectively (steps starting at −225 pA with 50 pA increments; duration, 1 s). Arrow shows a sag that is often observed upon hyperpolarizing current injection in Type A and B cells. The asterisk in Ba indicates rebound burst spikes generated by negative current injection. A depolarizing current pulse of 125 pA (red trace) evoked repetitive spike discharges in Type A and B neurons. Note the faster spiking in Type B than in Type A. Scale bars, 0.2 s, 50 mV. (Ab) A depolarizing plateau potential was evoked upon release from depolarizing current injection in 42.9% of the Type A neurons examined (arrow), but did not occur in Type B neurons. (Bb) Spontaneous spike discharges were frequently observed in Type B (77.0%), but only occasionally in Type A (17.0%) neurons. (C) Action potentials of Type A (black) and Type B (red) neurons. Scale bars, 2 ms, 20 mV. (D) Current–voltage relationships of EGFP-TH$^+$ Type A and B neurons. Error bars indicate SEM unless otherwise noted. $^*P < 0.05$, $^{**}P < 0.01$ for Type A neurons. (E) Decision boundary generated with discriminant analysis showing the distribution of EGFP$^+$ neurons. Individual neurons are plotted in two-dimensional space, where x- and y-axes represent resting membrane potential and spike width at half amplitude, respectively. White and red circles indicate EGFP-TH$^+$ Type A and B neurons, respectively. The Mahalanobis boundary, generated with discriminant analysis, is superimposed in the figure (black). The boundary ($x^2 + 753.64y^2 - 33.95xy + 143.09x - 3030.43y + 5137.58 = 0$) can be used to predict group membership of newly recorded cells by plotting their parameters and determining the territory into which they fall.

TABLE 1. Electrophysiological properties of two types of EGFP-positive neurons in the striatum

	EGFP-TH$^+$ Type A (n = 131)	EGFP-TH$^+$ Type B (n = 37)
Resting membrane potential (mV)	−76.0 ± 0.9	−65.3 ± 0.8**
Spike threshold (mV)	−51.0 ± 0.5	−49.2 ± 0.6*
Spike peak (mV)	27.0 ± 1.0	20.1 ± 1.8**
Spike amplitude (mV)	78.0 ± 1.2	69.3 ± 1.7**
Spike width at half amplitude (ms)	1.51 ± 0.05	0.68 ± 0.03**
Time to peak of AHP (ms)	29.0 ± 1.4	3.4 ± 0.5**
AHP amplitude (mV)	11.6 ± 0.5	15.5 ± 0.8**
Input resistance (MW)	406 ± 22	635 ± 54**

Data are mean ± SE. Time to peak and amplitude of afterhyperpolarization (AHP) were measured from the spike onset. *P < 0.05, **P < 0.01.

contributed to the separation of these groups. Among many pairs of variables, we chose resting membrane potential and spike width at half amplitude, which maximized accuracy (Wilks' lambda, 0.368; F value, 126.04; P < 0.01). The correction rate was 100% for both EGFP-TH$^+$ Type A and Type B neurons (113/113 for EGFP-TH$^+$ Type A and 37/37 for Type B) (Fig. 5E). As the assumption of homogeneity of variance–covariance matrices was violated, discriminant analysis using Mahalanobis distances (Mahalanobis, 1936) was used. When x and y denoted resting membrane potential and spike width at half amplitude, respectively, the Mahalanobis boundary generated with discriminant analysis was $x^2 + 753.64y^2 - 33.95xy + 143.09x - 3030.43y + 5137.58 = 0$.

Morphological analysis of EGFP-TH$^+$ Type A and Type B neurons

The electrophysiologically classified EGFP-TH$^+$ Type A and Type B neurons were also histologically unique. To test whether EGFP-TH$^+$ Type A and Type B neurons also exhibited morphological differences, neurons were labeled with biocytin, reconstructed and projected to a coronal plane. EGFP-TH$^+$ Type A neurons consisted of aspiny and spiny neurons, with the majority being aspiny (75.4%, 46/61) (Fig. 6A). Although the longest dendrite of the spiny type was significantly longer than the aspiny Type A neurons (aspiny, 104.2 ± 6.3 μm; spiny, 141.8 ± 9.0 μm; P < 0.01), we did not find any significant differences between them in other basic morphological and electrophysiological parameters, including soma area (aspiny, 82.5 ± 3.9 μm^2; spiny, 91.9 ± 6.6 μm^2; P > 0.2), number of primary dendrites (aspiny, 4.9 ± 0.3; spiny, 5.2 ± 0.3; P > 0.5), resting membrane potential (aspiny, −60.8 ± 1.7 mV; spiny, −61.4 ± 2.3 mV; P > 0.8) and input resistance (aspiny, 381 ± 33 MΩ; spiny, 470 ± 55 MΩ; P > 0.1). Therefore, we grouped these data together in the following analysis. Fifteen EGFP-TH$^+$ Type B neurons were recovered from a total of 74 EGFP-TH$^+$ neurons. The number of primary dendrites ranged from 2 to 9 in Type A and from 2 to 4 in Type B neurons, with Type A neurons having more primary dendrites than Type B neurons (Type A, 4.4 ± 0.2; Type B, 3.2 ± 0. 2; P < 0.01, Fig. 6B). In both Type A and B cells, fine axon collaterals were branched within the striatum directly from the soma or primary dendrite (Fig. 6A, red). However, we could not determine whether the axon fibers projected to the extrastriatal regions because of the limitation in our slice preparations. With respect to the soma areas, no significant difference was found between Type A and B neurons (Type A, 90.2 ± 3.3 μm^2, n = 61; Type B, 101.5 ± 5.7 μm^2, n = 13), with the soma areas being similar to those of MSNs (n = 22). However, they were significantly smaller than those of interneurons, such as cholinergic giant aspiny interneurons (long-afterhyperpolarization cell, n = 16), somatostatin/nitric oxide synthase/neuropeptide Y-containing aspiny GABA interneurons (low-threshold spike cell, n = 12) and parvalbumin-containing GABA aspiny interneurons (fast-spiking cell, n = 15) ($F_{5,210}$ = 58.255, P < 0.001) (Fig. 6C). As Type A neurons had spines in 46/61 cells at P18, we tried to compare the spines of

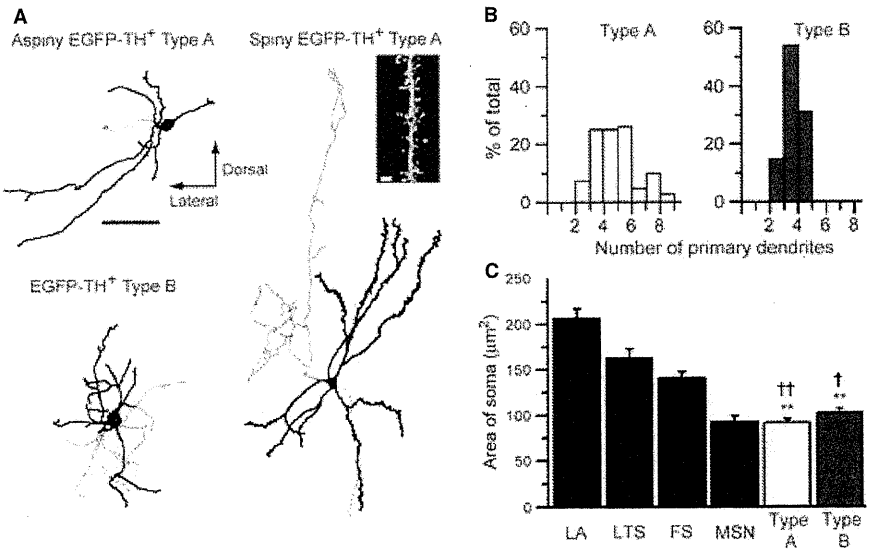

FIG. 6. Morphological features of EGFP-TH$^+$ Type A and B neurons. (A) Examples of camera lucida reconstructions displaying the morphology of aspiny EGFP-TH$^+$ Type A, spiny Type A and aspiny Type B neurons. Somata and dendritic trees are drawn in black and the axons in red. The inset shows a high-magnification micrograph of a dendritic segment of the spiny Type A neuron. The dendrites are densely studded with spines. (B) Frequency distribution of primary dendrites of EGFP-TH$^+$ Type A and B neurons. The number of primary dendrites of Type A and Type B neurons ranged from 2 to 9 and from 2 to 4, respectively. Type A neurons had more primary dendrites than Type B neurons (Type A neuron, 4.4 ± 0.2; Type B neuron, 3.2 ± 0. 2; P < 0.01). (C) Comparison of soma areas of long-afterhyperpolarization cell (LA), low-threshold spike cell (LTS), fast-spiking cell (FS), MSN, Type A and Type B neurons. There is no difference among the soma areas of MS, Type A and Type B neurons. Scale bar: A, 50 μm; inset, 2 μm. **P < 0.01 for LA and LTS neurons, $^{\dagger}P$ < 0.05, $^{\dagger\dagger}P$ < 0.001 for FS neurons.

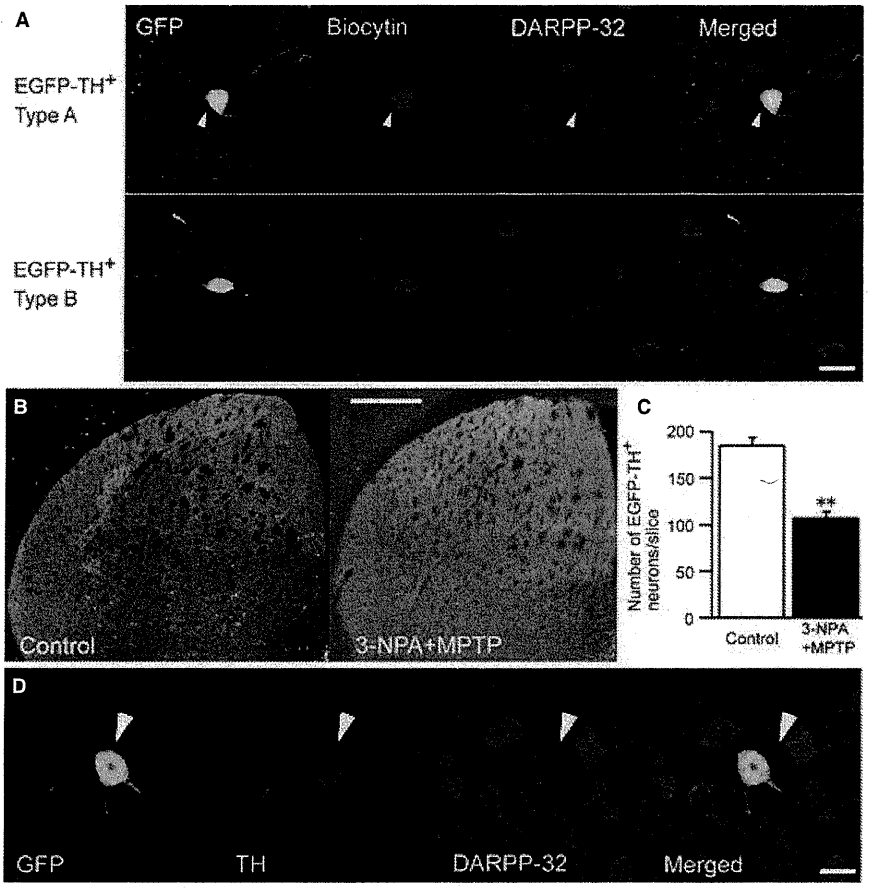

FIG. 7. EGFP-TH$^+$ Type A neurons are DARPP-32-positive and express TH immunoreactivity after dopamine depletion. (A) DARPP-32 staining of biocytin-filled EGFP$^+$ neurons after electrophysiological recordings revealed that EGFP-TH$^+$ Type A neurons were colocalized with DARPP-32. In contrast, Type B neurons were immunonegative for DARPP-32. Arrowheads indicate a triple-labeled neuron. Scale bar: 10 μm. (B–D) Effect of a combined treatment of 3-NPA and MPTP on EGFP$^+$ neurons in the striatum. (B) EGFP$^+$ neurons (white dots) are scattered in the striatum of a control mouse but much less abundantly in the 3-NP+MPTP-treated mouse. (C) Effect of the combined treatment of 3-NPA and MPTP on the number of EGFP$^+$ neurons in the striatum. The treatment significantly decreased the number of EGFP$^+$ neurons. (D) Phenotypic characterization of TH-immunoreactive neurons in the striatum of the 3-NP+MPTP-treated mouse. Fluorescent labeling of green fluorescent protein (GFP, green), TH (red) and DARPP-32 (blue) is merged to show a triple-labeled neuron (Merged, arrowhead). A DARPP-32-positive EGFP$^+$ neuron shows TH immunoreactivity after the treatment. Scale bar: A and D, 10 μm; B, 500 μm. $^{**}P < 0.01$.

EGFP-TH$^+$ neurons and those of MSNs in younger mice. We found dendritic spines in all of the seven MSNs recovered and in six out of 15 EGFP-TH$^+$ Type A neurons, even at P7–11. Dendritic spines in MSNs seemed to be more numerous and thicker than those in Type A neurons. However, it was difficult to detect such subtle differences under an optical microscope from a small sample of cells.

DARPP-32-immunoreactive EGFP-TH$^+$ neurons express tyrosine hydroxylase immunoreactivity after dopamine depletion

Remarkably, EGFP-TH$^+$ Type A and Type B neurons corresponded very well to DARPP-32-positive (six out of eight Type A neurons) and DARPP-32-negative (two out of two Type B neurons) EGFP-TH$^+$ neurons, respectively (Fig. 7A). DARPP-32 is a well-known marker for MSNs (Anderson & Reiner, 1991; Ouimet *et al.*, 1998), indicating that EGFP-TH$^+$ Type A neurons and MSNs resemble each other in this sense.

To determine which of the EGFP-TH$^+$ neurons express TH protein after 3-NPA and MPTP treatment, the drugs were administered to 2-month-old EGFP-TH$^+$ transgenic mice. It was reported previously that combined treatment with 3-NPA and MPTP successfully induced TH protein expression in the mouse striatum (Nakahara *et al.*, 2001). As it was reported that dopamine fiber denervation stimulated neurogenesis in the subventricular zone (Peng *et al.*, 2008), BrdU was also administered to assess the possibility of neurogenesis in our transgenic mouse. At 1 week after the last MPTP injection, brains were removed and fixed for immunohistochemistry. We found that the treatment significantly decreased the number of EGFP-positive neurons in the striatum (Fig. 7B and C), and concurrently induced TH expression in a small population of EGFP-TH$^+$ neurons (3.4%, 12/354). These TH-positive neurons were also immunostained for EGFP and DARPP-32 (Fig. 7D), suggesting that EGFP-TH$^+$ Type A neurons might have transformed into TH-immunoreactive neurons after dopamine denervation. There were no BrdU-labeled EGFP-positive neurons in the striatum, although BrdU labeled many small cells after 3-NPA and MPTP treatment (data not shown).

Comparison between EGFP-TH$^+$ Type A neurons and medium spiny neurons

The fact that EGFP-TH$^+$ Type A neurons and MSNs have a lot in common, such as the soma size, spiny dendrites, immunoreactivity for

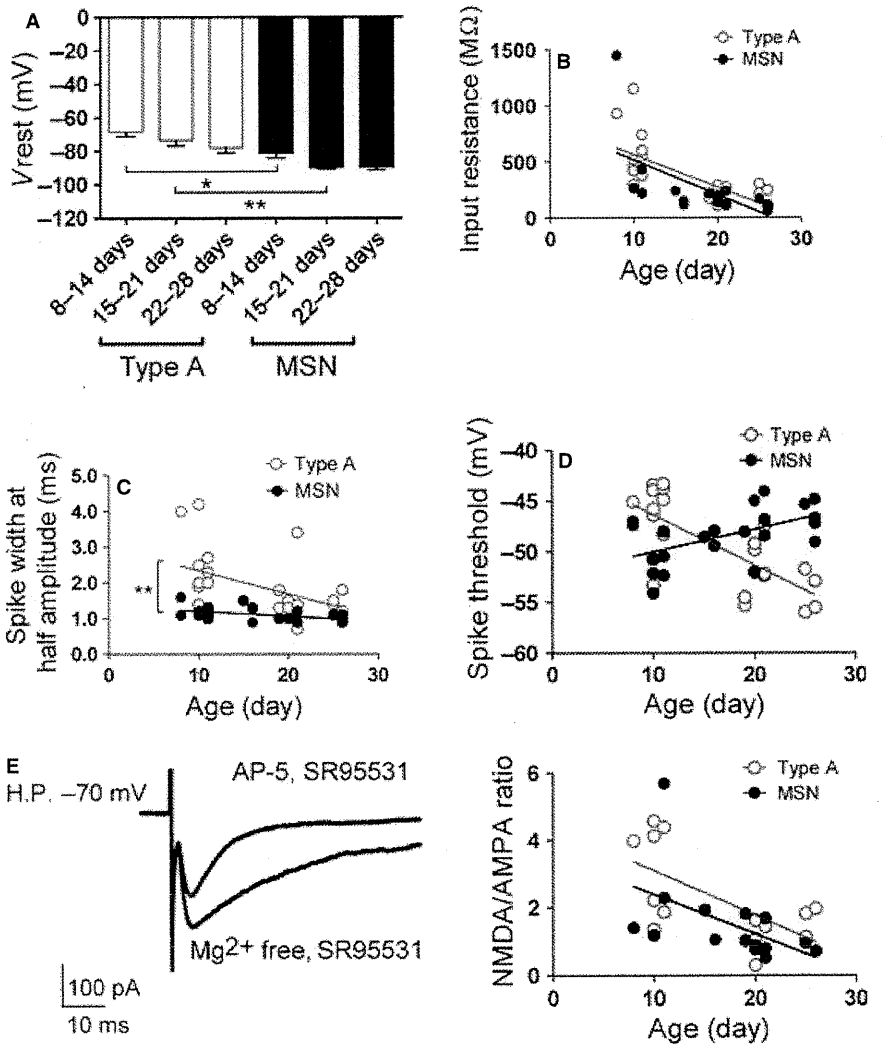

FIG. 8. Comparisons of the electrophysiological properties in EGFP-TH$^+$ Type A neurons and MSNs. (A) Resting membrane potentials (Vrest) of Type A cells during postnatal periods of 8–14, 15–21 and 22–28 days were more depolarized than those of MSNs of the same postnatal periods. $^*P < 0.05$, $^{**}P < 0.01$. (B) Input resistances of Type A neurons and MSNs tend to decrease during development in a similar manner. (C) Spike widths at half amplitude of Type A neurons, which were significantly shorter than those of MSNs during the 8- to 14-day period, tended to decrease to similar values to those of MSNs. $^{**}P < 0.01$. (D) There was no difference in the spike threshold between Type A neurons and MSNs throughout the development. (E) NMDA : non-NMDA ratios were measured as the area of EPSC (charge transfer) under the first 150 ms after the stimulus artifact. The control EPSC was recorded in magnesium-free saline containing the $GABA_A$ receptor antagonist SR-95531 (5 μM) and the non-NMDA current was sampled in the presence of D-(−)-2-amino-5-phosphonopentanic acid (AP-5) (25 μM) and SR-95531. The NMDA current was calculated by subtracting the non-NMDA current from the control EPSC. The NMDA : non-NMDA ratios of both Type A neurons and MSNs tended to decrease during development and there was no difference between the two. Holding potential (H.P.) was −70 mV.

DARPP-32 (as well as enkephalin and dynorphin) and the late appearance of calbindin immunoreactivity in DARPP-32-positive cells, led us to conduct a series of experiments to examine and compare the postnatal development of electrophysiological features of EGFP-TH$^+$ Type A neurons and MSNs using slices taken from P8 to P28 mice (Fig. 8). Resting membrane potentials of both cell types had a tendency to deepen and those of MSNs were significantly deeper than those of EGFP-TH$^+$ cells at P8–P21, but became similar from P22 onward [Type A: P8–14, −68.5 ± 2.6 mV (n = 14), P15–21, −73.5 ± 3.3 mV (n = 8), P22–28, −78.0 ± 2.9 mV (n = 4); MSN: P8–14, −81.0 ± 2.1 mV (n = 8), P15–21, −89.7 ± 1.0 mV (n = 9), P22–28, −89.5 ± 1.7 mV (n = 6); Type A vs. MSN: P8–14, $P < 0.05$, P15–21, $P < 0.01$, P22–28, not significant, Fig. 8A]. Input resistances of both cell types gradually decreased during postnatal development [Type A (n = 22), R^2 = 0.47; MSN (n = 19), R^2 = 0.38, Fig. 8B], and no difference was found between the two. Spike widths at half amplitude of EGFP-TH$^+$ cells at P8–14 were wider than those of MSNs at P8–14, but gradually decreased to values that were similar to those of MSNs [Type A: P8–14 (n = 11), 2.3 ± 0.3 ms, P15–21 (n = 8), 1.6 ± 0.3 ms, P22–28 (n = 4), 1.5 ± 0.1 ms; MSN: P8–14 (n = 8), 1.2 ± 0.1 ms, P15–21 (n = 9), 1.1 ± 0.1 ms, P22–28 (n = 5), 1.0 ± 0.0 ms; Type A vs. MSN: P8–14, $P < 0.01$, P15–28, not significant, Fig. 8C]. Spike thresholds of both cell types were similar to each other throughout (Fig. 8D). We next examined the postnatal development of the NMDA : non-NMDA ratios of EPSCs evoked by intrastriatal stimulation (Fig. 8E). The ratios of both cell types decreased similarly and no statistical differences were obtained throughout. Overall, the basic membrane properties of both cell types were very similar at P22–28, although some differences, such as resting membrane potentials and spike widths, were found early in development.

Discussion

In this study, using juvenile transgenic mice expressing EGFP under the control of the TH promoter, we showed that TH mRNA-expressing EGFP$^+$ neurons were GABAergic and mostly calbindin-negative, and could be classified immunohistochemically and electrophysiologically into at least two distinct neuronal types, EGFP-TH$^+$ Type A and Type B. Type B neurons had more depolarized resting membrane potentials and displayed higher frequency discharges with narrower spike half widths than Type A. They were DARPP-32-negative and contained calretinin GABAergic interneurons. Type A neurons were DARPP-32-positive, had mostly aspiny but occasionally spiny dendrites and made up a large majority of EGFP$^+$ neurons, thus resembling MSNs. They expressed TH immunoreactivity after a combined treatment of MPTP and 3-NPA, aimed at complete depletion of dopamine. Despite a close resemblance to MSNs, Type A neurons differ from MSNs in their lack of calbindin immunoreactivity, a lower incidence of spiny dendrites, disregard of striatal compartments and a distinct time course of postnatal development of electrophysiological and immunohistochemical properties.

Electrophysiological characterization of EGFP-TH$^+$ neurons

Electrophysiological characterization of EGFP-TH$^+$ neurons was recently made by Tepper and colleagues using adult bacterial artificial chromosome transgenic mice between 2 and 4 months of age, where at least four types of EGFP-TH$^+$ neurons termed Type I–IV were identified in the striatum (Ibanez-Sandoval *et al.*, 2010). The vast majority of the EGFP-TH$^+$ neurons in the adult bacterial artificial chromosome transgenic mouse were Type I neurons that had a high input resistance, a modest slow inward rectification to hyperpolarizing current injection, an action potential duration of 0.78 ms, a modest, voltage- and time-dependent sag in response to hyperpolarizing current injection, a marked spike frequency adaptation and a depolarizing plateau potential after depolarizing current pulse. The Type I neurons also contained cells that were 'densely invested with elongated, stick-like dendritic appendages'. These properties were very similar to those observed in our Type A neurons, which were found to be the most numerous, except that we encountered cells with more spine-like structures rather than the stick-like appendages as shown in Fig. 6. However, our Type B neurons seem to contain some features of the remaining Type II-IV neurons, such as a very short spike width at half amplitude (Type B neurons, 0.68 ms; Type II-IV neurons, 0.43–0.5 ms), a very high frequency discharge (Type II and IV) and rebound bursting after the offset of hyperpolarizing current injection (Type IV). However, depolarizing plateau potentials (Type III) after depolarizing current injections were only rarely observed in Type B neurons. These discrepancies may be derived from the difference in the transgenic mouse strain used in the experiments or, alternatively, the difference in age of the mice used (8–28 days old vs. 2–4 months old).

Tyrosine hydroxylase mRNA-containing neurons consist of at least two types of GABA neurons

More than 90% of the EGFP$^+$ neurons in the striatum showed immunoreactivity to GAD65/67, indicating that EGFP$^+$ Type A and B cells were GABAergic. Among four types of GABAergic neurons classically characterized in the striatum, none of the EGFP$^+$ neurons were immunopositive for parvalbumin and neuronal nitric oxide synthase, but 2.8% of them were colocalized with calretinin. Therefore, the calretinin-containing GABA interneurons may include these calretinin-positive EGFP$^+$ neurons. Although immunostaining of electrophysiologically identified Type B neurons with calretinin antibody was not successful (both were immunonegative for DARPP-32), it is suggested that they belong to the same neuronal subtype, or at least a DARPP-32-negative non-Type A subtype. In contrast, most of the Type A neurons at P18 contained DARPP-32 and were calbindin-negative. DARPP-32, the phosphorylation of which is regulated by dopamine and cAMP, is known to be expressed in dopaminoceptive MSNs (Ouimet *et al.*, 1998). Calbindin, a 28-kD calcium-binding protein, is also a marker for MSNs in the striatal matrix compartment, which is complementary to the patches or striosomes where μ-opioid receptor binding is dense and acetylcholinesterase and calbindin labeling are poor (Gerfen, 1992). Therefore, Type A neurons possess a superficial resemblance to MSNs in the striosomes; however, they are dispersed equally in the patch/striosome-matrix compartments during postnatal development, so that they appear to correspond to neither the MSNs nor the classical GABA interneurons mentioned above. Interestingly, using adult male C57/BL6 mice, Darmopil *et al.* (2008) found that, as early as 3 days after a 6-hydroxydopamine lesioning, TH-immunoreactive spiny neurons appeared that were colocalized with calbindin and dynorphin or enkephalin, all of which are markers for MSNs in the matrix. Whether relevant or irrelevant, we encountered a few calbindin-positive EGFP$^+$ neurons adjacent to the subventricular zone at 2 months of age, suggesting that some of the TH mRNA-expressing neurons might acquire calbindin-like immunoreactivity in the adult. Alternatively, calbindin protein levels in Type A neurons might be too low to be detected immunohistochemically under normal conditions, whereas dopaminergic neuronal lesions, and the concomitant uptake of L-DOPA, might up-regulate calbindin protein expression. Therefore, the question arises as to whether or not Type A neurons are MSNs.

Type A neurons and medium spiny neurons are very much alike yet different

Comparison of the postnatal development of the electrophysiological properties of Type A neurons and MSNs revealed, surprisingly, that they resembled each other from P22 onward in some membrane properties, but in others exhibited different developmental time courses. Specifically, resting membrane potentials and spike widths at half amplitude were significantly different between the two types of neurons at P8–14. In addition, examination of the postnatal development of major immunohistochemical properties important for the identification of MSNs, such as calbindin, DARPP-32 and dynorphin B, revealed significant differences between the two. Assuming that medium-sized neurons with round nuclei were MSNs and that EGFP$^+$-bright areas were dopamine islands, calbindin-poor and calbindin-rich zones were observed in the matrix at P2 but were obscure at P8, as pointed out by Liu & Graybiel (1992a,b). Notably, the percentage of medium-sized neurons with calbindin-like immunoreactivity was more than 80% in the dopamine islands at P2 and P8, but drastically decreased to less than 10% at P26, whereas calbindin-like immunoreactive cells in the matrix steadily increased from about 50% at P2 to more than 80% at P8 and 96.5% at P26. In contrast, calbindin-like immunoreactive EGFP-TH$^+$ neurons remained very low in number from P2 onward. DARPP-32-like immunoreactive cells were barely detectable at birth, but increased rapidly, peaking at P28, and then declined to plateau levels in the adult; this occurred independently of dopaminergic input from the substantia nigra (Ehrlich *et al.*, 1990).

Similarly, the number of cells with DARPP-32-like immunoreactivity in both dopamine islands and the matrix increased dramatically from about 10 and 46% at P2, respectively, to more than 90% at P26. In contrast, the percentage of DARPP-32-positive cells among the EGFP-TH$^+$ neurons remained high throughout development. We also examined whether EGFP-TH$^+$ neurons contained enkephalin (for the indirect pathway) or dynorphin B (for the direct pathway) at P18, and found that over half of the EGFP-TH$^+$ neurons exhibited immunoreactivity for enkephalin (30/55) and 80% of the cells contained dynorphin (56/70), as reported by Darmopil *et al.* (2008). Throughout the first three postnatal weeks, dynorphin B-like immunoreactivity was more frequently observed in EGFP-TH$^+$ neurons, as well as medium-sized cells in the dopamine islands, than cells in the matrix.

To sum up, Type A neurons are very similar to MSNs in the following respects. First, they have a similar somal size and a proportion have numerous dendritic spines. Second, they express specific markers for MSNs: DARPP-32, enkephalin and dynorphin. Third, the electrophysiological properties of Type A neurons resemble those of MSNs from P22 onward. Some cells even had delayed spiking due to a depolarizing ramp with modest inward rectification that characterizes MSNs. Conversely, Type A neurons differ from MSNs in that, first, they mostly lack calbindin and ignore striatal compartments. Second, only a quarter of Type A cells had spiny dendrites. Third, they exhibit a different time course of electrophysiological development. Fourth, the postnatal development of calbindin-like, DARPP-32-like and dynorphin B-like immunoreactivity of Type A neurons was significantly different from that of medium-sized neurons in the matrix. Fifth, a piece of evidence against the proposition that they are projection neurons has been provided. Ibanez-Sandoval *et al.* (2010) found that no EGFP-TH$^+$ neurons were retrogradely labeled by bilateral injection of rhodamine beads into the globus pallidus and substantia nigra. Similarly, we did not find any biocytin-filled Type A cells emitting axons outside the striatum in a slice preparation. We therefore conclude that Type A neurons and MSNs may be of the same origin and are very much alike, yet are distinct from each other. Therefore, were all of the TH-positive cells appearing after dopamine depletion derived from EGFP-TH neurons? It is natural to think that the EGFP-TH$^+$ neurons should begin to produce detectable levels of TH after dopamine depletion, as they possess TH mRNA and occasionally express weak TH immunoreactivity in a physiological situation (data not shown), but strong TH immunostaining in response to colchicine administration (Ibanez-Sandoval *et al.*, 2010). As such, another possibility of MSNs becoming TH-expressing neurons cannot be ruled out. MSNs do not contain detectable levels of TH mRNA under physiological conditions. However, as demonstrated by Darmopil *et al.* (2008), a combined treatment of 6-hydroxydopamine injection and L-DOPA intake might have caused MSNs to recruit or up-regulate TH mRNA and protein, and produce dopamine via L-DOPA, so that TH-expressing neurons might have been found to be indistinguishable from MSNs (Huot & Parent, 2007). A more thorough investigation of the physiological properties of dopamine-producing neurons in the striatum is certainly needed to utilize these neurons to alleviate or compensate for symptoms of Parkinson's disease.

Acknowledgements

We would like to thank Fusae Nagumo for her technical support. This study was supported by grants from the Ministry of Education, Culture, Sports, Science and Technology of Japan, Japan Society for the Promotion of Science and the Smoking Research Foundation of Japan.

Abbreviations

BrdU, bromodeoxyuridine; DARPP-32, dopamine- and cyclic AMP-regulated phosphoprotein of 32 kDa; EGFP, enhanced green fluorescent protein; EPSC, excitatory postsynaptic current; GAD, glutamic acid decarboxylase; MPTP, 1-methyl-4-phenyl-1,2,3,6-tetrahydropyridine; MSN, medium spiny neuron; NMDA, *N*-methyl-D-aspartate; P, postnatal day; PBS, phosphate-buffered saline; TH, tyrosine hydroxylase; 3-NPA, 3-nitropropionic acid.

References

Anderson, K.D. & Reiner, A. (1991) Immunohistochemical localization of DARPP-32 in striatal projection neurons and striatal interneurons: implications for the localization of D1-like dopamine receptors on different types of striatal neurons. *Brain Res.*, **568**, 235–243.

Baker, H., Kobayashi, K., Okano, H. & Saino-Saito, S. (2003) Cortical and striatal expression of tyrosine hydroxylase mRNA in neonatal and adult mice. *Cell. Mol. Neurobiol.*, **23**, 507–518.

Betarbet, R., Turner, R., Chockkan, V., DeLong, M.R., Allers, K.A., Walters, J., Levey, A.I. & Greenamyre, J.T. (1997) Dopaminergic neurons intrinsic to the primate striatum. *J. Neurosci.*, **17**, 6761–6768.

Cossette, M., Levesque, D. & Parent, A. (2005) Neurochemical characterization of dopaminergic neurons in human striatum. *Parkinsonism. Relat. Disord.*, **11**, 277–286.

Darmopil, S., Muneton-Gomez, V.C., de Ceballos, M.L., Bernson, M. & Moratalla, R. (2008) Tyrosine hydroxylase cells appearing in the mouse striatum after dopamine denervation are likely to be projection neurones regulated by L-DOPA. *Eur. J. Neurosci.*, **27**, 580–592.

Dubach, M., Schmidt, R., Kunkel, D., Bowden, D.M., Martin, R. & German, D.C. (1987) Primate neostriatal neurons containing tyrosine hydroxylase: immunohistochemical evidence. *Neurosci. Lett.*, **75**, 205–210.

Ehrlich, M.E., Rosen, N.L., Kurihara, T., Shalaby, I.A. & Greengard, P. (1990) DARPP-32 development in the caudate nucleus is independent of afferent input from the substantia nigra. *Brain Res. Dev. Brain Res.*, **54**, 257–263.

Francis, F., Koulakoff, A., Boucher, D., Chafey, P., Schaar, B., Vinet, M.C., Friocourt, G., McDonnell, N., Reiner, O., Kahn, A., McConnell, S.K., Berwald-Netter, Y., Denoulet, P. & Chelly, J. (1999) Doublecortin is a developmentally regulated, microtubule-associated protein expressed in migrating and differentiating neurons. *Neuron*, **23**, 247–256.

Gerfen, C.R. (1992) The neostriatal mosaic: multiple levels of compartmental organization in the basal ganglia. *Annu. Rev. Neurosci.*, **15**, 285–320.

Gerfen, C.R. & Young, W.S. 3rd (1988) Distribution of striatonigral and striatopallidal peptidergic neurons in both patch and matrix compartments: an in situ hybridization histochemistry and fluorescent retrograde tracing study. *Brain Res.*, **460**, 161–167.

Gerfen, C.R., Baimbridge, K.G. & Miller, J.J. (1985) The neostriatal mosaic: compartmental distribution of calcium-binding protein and parvalbumin in the basal ganglia of the rat and monkey. *Proc. Natl. Acad. Sci. USA*, **82**, 8780–8784.

Huot, P. & Parent, A. (2007) Dopaminergic neurons intrinsic to the striatum. *J. Neurochem.*, **101**, 1441–1447.

Ibanez-Sandoval, O., Tecuapetla, F., Unal, B., Shah, F., Koos, T. & Tepper, J.M. (2010) Electrophysiological and morphological characteristics and synaptic connectivity of tyrosine hydroxylase-expressing neurons in adult mouse striatum. *J. Neurosci.*, **30**, 6999–7016.

Ikemoto, K., Kitahama, K., Jouvet, A., Arai, R., Nishimura, A., Nishi, K. & Nagatsu, I. (1997) Demonstration of L-dopa decarboxylating neurons specific to human striatum. *Neurosci. Lett.*, **232**, 111–114.

Jinno, S. & Kosaka, T. (2004) Parvalbumin is expressed in glutamatergic and GABAergic corticostriatal pathway in mice. *J. Comp. Neurol.*, **477**, 188–201.

Jollivet, C., Montero-Menei, C.N., Venier-Julienne, M.C., Sapin, A., Benoit, J.P. & Menei, P. (2004) Striatal tyrosine hydroxylase immunoreactive neurons are induced by L-dihydroxyphenylalanine and nerve growth factor treatment in 6-hydroxydopamine lesioned rats. *Neurosci. Lett.*, **362**, 79–82.

Kawaguchi, Y., Wilson, C.J., Augood, S.J. & Emson, P.C. (1995) Striatal interneurones: chemical, physiological and morphological characterization. *Trends Neurosci.*, **18**, 527–535.

Liu, F.C. & Graybiel, A.M. (1992a) Heterogeneous development of calbindin-D28K expression in the striatal matrix. *J. Comp. Neurol.*, **320**, 304–322.

Liu, F.C. & Graybiel, A.M. (1992b) Transient calbindin-D28k-positive systems in the telencephalon: ganglionic eminence, developing striatum and cerebral cortex. *J. Neurosci.*, **12**, 674–690.

Lopez-Real, A., Rodriguez-Pallares, J., Guerra, M.J. & Labandeira-Garcia, J.L. (2003) Localization and functional significance of striatal neurons

immunoreactive to aromatic L-amino acid decarboxylase or tyrosine hydroxylase in rat Parkinsonian models. *Brain Res.*, **969**, 135–146.

Mahalanobis, P.C. (1936) On the generalized distance in statistics. *Proc. Natl. Inst. Sci. (India)*, **12**, 49–55.

Mao, L., Lau, Y.S., Petroske, E. & Wang, J.Q. (2001) Profound astrogenesis in the striatum of adult mice following nigrostriatal dopaminergic lesion by repeated MPTP administration. *Brain Res. Dev. Brain Res.*, **131**, 57–65.

Matsushita, N., Okada, H., Yasoshima, Y., Takahashi, K., Kiuchi, K. & Kobayashi, K. (2002) Dynamics of tyrosine hydroxylase promoter activity during midbrain dopaminergic neuron development. *J. Neurochem.*, **82**, 295–304.

Mura, A., Linder, J.C., Young, S.J. & Groves, P.M. (2000) Striatal cells containing aromatic L-amino acid decarboxylase: an immunohistochemical comparison with other classes of striatal neurons. *Neuroscience*, **98**, 501–511.

Nacher, J., Crespo, C. & McEwen, B.S. (2001) Doublecortin expression in the adult rat telencephalon. *Eur. J. Neurosci.*, **14**, 629–644.

Nakahara, T., Yamamoto, T., Endo, K. & Kayama, H. (2001) Neuronal ectopic expression of tyrosine hydroxylase in the mouse striatum by combined administration of 1-methyl-4-phenyl-1,2,3,6-tetrahydropyridine and 3-nitropropionic acid. *Neuroscience*, **108**, 601–610.

Nery, S., Fishell, G. & Corbin, J.G. (2002) The caudal ganglionic eminence is a source of distinct cortical and subcortical cell populations. *Nat. Neurosci.*, **5**, 1279–1287.

Ouimet, C.C., Langley-Gullion, K.C. & Greengard, P. (1998) Quantitative immunocytochemistry of DARPP-32-expressing neurons in the rat caudatoputamen. *Brain Res.*, **808**, 8–12.

Palfi, S., Leventhal, L., Chu, Y., Ma, S.Y., Emborg, M., Bakay, R., Deglon, N., Hantraye, P., Aebischer, P. & Kordower, J.H. (2002) Lentivirally delivered glial cell line-derived neurotrophic factor increases the number of striatal dopaminergic neurons in primate models of nigrostriatal degeneration. *J. Neurosci.*, **22**, 4942–4954.

Peng, J., Xie, L., Jin, K., Greenberg, D.A. & Andersen, J.K. (2008) Fibroblast growth factor 2 enhances striatal and nigral neurogenesis in the acute 1-methyl-4-phenyl-1,2,3,6-tetrahydropyridine model of Parkinson's disease. *Neuroscience*, **153**, 664–670.

Porritt, M.J., Batchelor, P.E., Hughes, A.J., Kalnins, R., Donnan, G.A. & Howells, D.W. (2000) New dopaminergic neurons in Parkinson's disease striatum. *Lancet*, **356**, 44–45.

Sawamoto, K., Nakao, N., Kobayashi, K., Matsushita, N., Takahashi, H., Kakishita, K., Yamamoto, A., Yoshizaki, T., Terashima, T., Murakami, F., Itakura, T. & Okano, H. (2001) Visualization, direct isolation, and transplantation of midbrain dopaminergic neurons. *Proc. Natl. Acad. Sci. USA*, **98**, 6423–6428.

Tande, D., Hoglinger, G., Debeir, T., Freundlieb, N., Hirsch, E.C. & Francois, C. (2006) New striatal dopamine neurons in MPTP-treated macaques result from a phenotypic shift and not neurogenesis. *Brain*, **129**, 1194–1200.

Tashiro, Y., Kaneko, T., Sugimoto, T., Nagatsu, I., Kikuchi, H. & Mizuno, N. (1989a) Striatal neurons with aromatic L-amino acid decarboxylase-like immunoreactivity in the rat. *Neurosci. Lett.*, **100**, 29–34.

Tashiro, Y., Sugimoto, T., Hattori, T., Uemura, Y., Nagatsu, I., Kikuchi, H. & Mizuno, N. (1989b) Tyrosine hydroxylase-like immunoreactive neurons in the striatum of the rat. *Neurosci. Lett.*, **97**, 6–10.

Yang, H.K., Sundholm-Peters, N.L., Goings, G.E., Walker, A.S., Hyland, K. & Szele, F.G. (2004) Distribution of doublecortin expressing cells near the lateral ventricles in the adult mouse brain. *J. Neurosci. Res.*, **76**, 282–295.

連載
第13回
気になる脳部位

視床下核

南部　篤

自然科学研究機構生理学研究所生体システム研究部門

はじめに

視床下核（subthalamic nucleus）はその名のとおり，視床の下に存在する紡錘形の小さな核（ヒトでは大粒の大豆大）であり，大脳基底核を構成する核の一つである（図1）[1]．Jules Bernard Luys が1865年に初めて記載したことからルイ体（corpus Luysi）ともよばれる[2]．視床下核の障害により反対側にヘミバリスム（hemiballism）が起こることが1920年代に明らかになり，注目されても良い筈であったが，長年，大脳基底核を巡る神経回路の中で，位置づけがはっきりせず，研究もあまり進んでいなかった．しかし，1990年に直接路・間接路モデルが提唱され，さらにパーキンソン病に対する定位脳手術（stereotactic surgery）のターゲットになってからは研究も進み，気になる脳部位の一つとなっている．

視床下核の位置づけ

以前は，視床下核は淡蒼球外節（external segment of the globus pallidus）と局所的な神経回路を構成しているだけであり，大脳基底核全体の情報処理とは無関係と考えられていた[3]．また，現在では，視床下核ニューロ

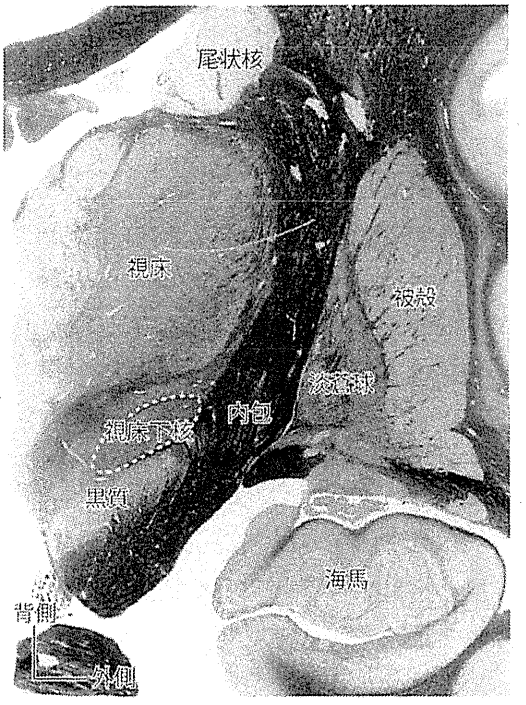

図1．ヒトの視床下核
ヒト脳の前額断切片（ヴァイゲルト髄鞘染色）で，視床下核を白破線で囲って示す．
（Mai JK *et al*, 2008[3]．http://www.thehumanbrain.info より引用）

Key Words
・視床下核
・ヘミバリスム
・間接路
・ハイパー直接路
・パーキンソン病
・DBS

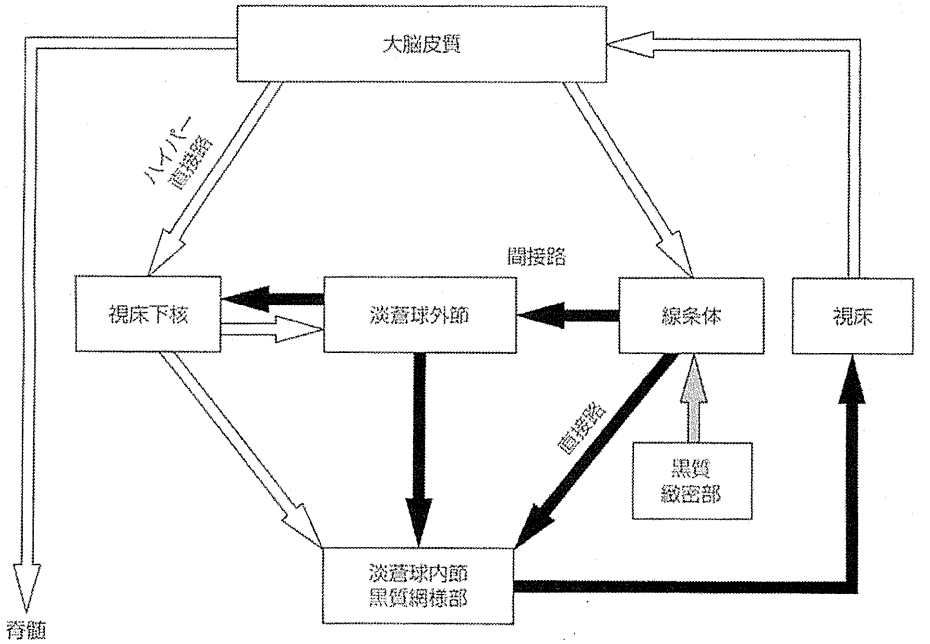

図 2. 大脳基底核を巡る神経回路
興奮性投射を白い矢印（⇨），抑制性投射を黒い矢印（➡），ドパミン作動性投射を灰色の矢印（➡）で示す．

（Nambu A *et al*, 2002[7]より改変引用）

ンは，グルタミン酸作動性の興奮性であることが確立しているが，抑制性であると考えられていた時期もあった．ところが1989年から1990年にかけてAlbinら[4]およびDeLongら[5]のグループによって，直接路・間接路モデルが提案され，状況が大きく変わった（図2）．彼らは，大脳基底核のうち入力部として線条体（striatum）を，出力部として淡蒼球内節（internal segment of the globus pallidus）と黒質網様部（substantia nigra pars reticulata）を定義し，入力部と出力部を以下の2つの経路が結ぶことを提案した．①直接路（direct pathway）：線条体から直接，淡蒼球内節・黒質網様部に到る経路．②間接路（indirect pathway）：線条体から，淡蒼球外節，視床下核を順に経由して淡蒼球内節・黒質網様部に到る経路．直接路・間接路モデルは，それまで入り組んでいた大脳基底核の神経回路を，整理し明快にまとめたばかりでなく，後から述べるように大脳基底核疾患の病態や定位脳手術の治療メカニズムも説明できる画期的なものであった．これによって，視床下核は間接路の重要な中継核と位置づけられた．

さらに，視床下核も大脳皮質から直接，入力を受けていることが以前よりわかっていたが，最近では大脳皮質からの入力が特に重要という認識が広がり，線条体とならんで大脳基底核の入力部と考えられるようになった．それに伴い，直接路・間接路に加えて，ハイパー直接路（hyperdirect pathway）：大脳皮質から入力を受けた視床下核ニューロンが淡蒼球内節・黒質網様部に投射する経路が提案され，広く認められるようになってきた（図2）[6,7]．

大脳基底核の入力部としての視床下核

視床下核には大脳皮質の各領野から投射があり，その背側部は，大脳皮質運動野から体部位局在を保った入力を受けていることから，運動領域と考えられる（図3）[8,9]．大脳皮質一次運動野からは視床下核背側部のうち外側部に，補足運動野からは内側部に投射している．一次運動野の口腔顔面，上肢，下肢領域からは視床下核外側部において，外側から内側にかけて終止しているのに対し，補足運動野の口腔顔面，上肢，下肢領域からの投射は，内側部において内側から外側に終止している．すなわち，外側部，内側部それぞれに，互いに鏡像関係にあるような体部位再現がある（図3）．この運動領域の腹側

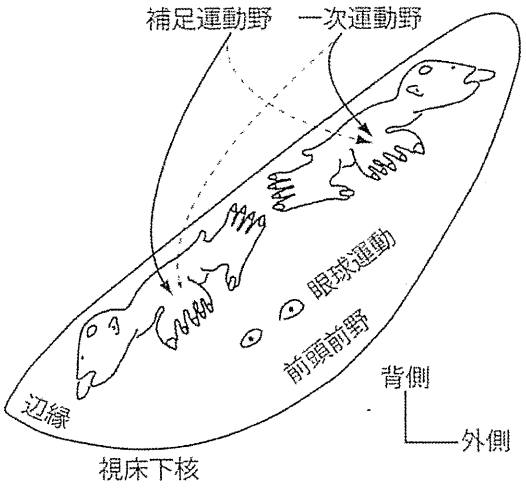

図 3. 視床下核の機能分化
視床下核を前額断で模式的に示す．視床下核背側部のうち，外側部は一次運動野から，内側部は補足運動野から，体部位局在を保った投射を受けている．一部，一次運動野から内側部に，補足運動野から外側部にも投射する．運動領域の腹側には前頭前野領域と，その一部に眼球運動領域が，最内側部には辺縁領域が存在する．
(Nambu A, 2011[9]より改変引用)

には前頭前野から，その一部に眼球運動野から，最内側部には辺縁皮質から入力を受ける領域が存在する．したがって，視床下核は上下肢や体幹の運動だけではなく，眼球運動，前頭前野の機能である高次機能，辺縁系の機能である情動などにもかかわっていると考えられる．

視床下核の機能

視床下核から神経活動を記録してみると，20～30 Hzの中程度の頻度でつねに発火しており，運動領域のニューロンは，反対側の対応する体部位の随意運動に先行して，活動を変化させることがわかる[10]．一方，視床下核はグルタミン酸作動性の興奮性ニューロンより構成されているので，投射先である淡蒼球外節・内節ニューロンに対して興奮性入力を与え，いわば大脳基底核のdriving forceとなっている．実際，視床下核を破壊したりブロックしたりすると，淡蒼球外節・内節のニューロン活動は減少する[9]．それに伴って，反対側に粗大な不随意運動であるヘミバリスムが出現する．これは，通常，ハイパー直接路や間接路が不必要な運動を抑制しているが，視床下核をブロックすると，不必要な運動を抑えられなくなり，不随意運動をきたしたと解釈できる．

大脳基底核疾患との関連

直接路・間接路モデルが広く受け入れられた理由として，大脳基底核疾患の病態が，直接路と間接路のバランスの崩れで説明できることにあった[5]．パーキンソン病の際には，線条体におけるドパミンの枯渇により，直接路ニューロンの活動性低下，間接路ニューロンの活動性亢進が想定され，それに伴って，淡蒼球内節の活動性亢進，淡蒼球外節の活動性低下，視床下核の活動性亢進が観察された[11]．さらに直接路・間接路モデルによると，活動性が亢進した視床下核を破壊すれば，パーキンソン病の症状が改善するはずであり，実際，動物実験で行ったところ，症状が軽減された[12]．これらが根拠となり，今日のような視床下核をターゲットとした定位脳手術の隆盛を見ることとなった．実際は，手技上の問題から視床下核を凝固するのではなく，視床下核に電極を挿入し高頻度電気刺激を加える脳深部刺激療法（deep brain stimulation：DBS）を行っている訳であるが[13]，これが局所の神経活動を抑制しているのか，興奮させているのか，いまだに議論があるところである[14]．さらに，当初，直接路と間接路の活動性のアンバランスを支持するデータが多かったが，その後の報告によれば，それほど明確ではなく，最近ではむしろ視床下核で観察される発振現象（β帯域のニューロン発火や局所フィールド電位）が，大脳基底核の情報伝達を阻害することにより，諸症状を引き起こしているのではないかとも考えられている[15]．

一方，DBSの副作用として，情動異常があげられる[13]．DBSは，視床下核の運動領域である背側部をターゲットとしているが，何らかの原因で電気刺激がより腹側部の前頭前野領域や辺縁領域にもおよび（図3），通常は視床下核の活動によって抑制されている情動機能が，DBSによって解放されたためではないかと考えられる．

おわりに

この20年間で，大脳基底核のうち視床下核ほど，見